

Anelastic Behavior of Suspension Plasma Sprayed Ceramic Coatings

Omid Rezaia

A Thesis

In

The Department

Of

Mechanical and Industrial Engineering

Presented in Partial Fulfillment of the Requirements
For the Degree of Master of Applied Science (Mechanical Engineering) at
Concordia University
Montreal, Quebec, Canada

Summer 2016

© Omid Rezaia 2016

Concordia University

CONCORDIA UNIVERSITY
School of Graduate Studies

This is to certify that the thesis prepared

By: Omid Rezanian

Entitled: Anelastic Behavior of Suspension Plasma Sprayed Ceramic Coatings

and submitted in partial fulfillment of the requirements for the degree of

Master of Applied Science (Mechanical Engineering)

complies with the regulations of the University and meets the accepted standards with respect to originality and quality.

Signed by the final examining committee:

M. Paraschivoiu Chair

A. Dolatabadi

A. Michael Zsaki Examiner

C. Moreau Supervisor

Approved by _____
Chair of Department or Graduate Program Director

Dean of Faculty

Date _____

Abstract

Suspension plasma spraying (SPS) is a rising coating technology producing fine nanostructured coatings with promising mechanical and physical properties while taking advantages of the well-established Atmospheric Plasma Spray (APS) process. Anelastic behavior of the coatings can be a specific identifier of their mechanical behavior which is related to the strength of coatings interlayers bonding and defect architecture. To better understand the relationship between SPS conditions and anelastic responses, post-deposition characterization technique under multiple thermal cycles using ex-situ coating property (ECP) sensor, which is based on thermal mismatch strain of coating-substrate system is applied. This technique makes it possible to determine the elastic modulus, non-linear degree and hysteresis degree of the spray coatings through the curvature-temperature response in a dependable and repeatable way. In this work, suspension plasma-sprayed YSZ ceramic coatings are produced under different spray conditions, and their anelastic characteristics are compared. The results show that the samples coated in high plasma power condition have a higher elastic modulus at low strain which is attributed to better inter-splat/inter-layer bonding due to higher particle impact velocity and temperature. However, samples produced in low raster speed condition have a relatively lower elastic modulus and higher compliance at an elevated temperature which describes the higher flexibility of these coating at higher temperature. These results make it possible to better understand the relationship between sprayed coating microstructures and mechanical properties in SPS coatings.

Acknowledgments

I would like to express my sincere gratitude to my supervisor, Prof. Christian Moreau, for his professional guidance and continuous encouragement throughout my thesis work. It has been my great honor and privilege to work under his supervision. He consistently allowed this research to be my own work but steered me in the right the direction whenever he thought I needed it.

I am also thankful to all members of thermal spray group at Concordia University. A very special thanks go out to Dr. Fadhel Ben Ettouil who assisted me a lot with my research. Also, I would like to thank my colleges Navid Sharifi, Maniya Aghasibeig, Ali Nozari, Alexandre Romão, Alexandre Laroche who supported and helped me with their knowledge and experience.

A very special thanks go out to all members of the center of thermal spray at Stony Brook University, NY, USA who provided me access to the laboratory and research facilities. Without they precious support, it would not have been possible to conduct this research.

Last but not the least, I would like to thank my family, especially my beautiful mother and my beloved father, and also my brother for supporting me spiritually throughout writing this thesis and my life in general. This accomplishment would not have been possible without them. Thank you.

Contents

1. Introduction and literature review	1
1.1. Suspension Plasma Spray process	4
1.2. Improved microstructure of thermal barrier coating (TBC) provided by submicron particles.....	6
1.3. Microstructural features of suspension plasma sprayed TBCs	8
1.4. Anelastic behavior in plasma sprayed ceramic coating.....	10
1.4.1. Background	10
1.5. Evaluation of anelastic behavior of plasma sprayed ceramic coating through Bi-layer Curvature-temperature (BCT) method	13
1.6. Objectives.....	17
2. Experimental procedures	18
2.1. Substrate Preparation.....	19
2.2. Suspension preparation and characterization.....	19
2.3. Procedure of suspension plasma spray process.....	22
2.3.1. Plasma generation.....	22
2.3.2. Suspension feeding mechanism.....	23
2.3.3. Coating deposition and torch raster pattern	24
2.3.4. Design of experiments for suspension plasma spray process	26
2.4. Coatings characterization.....	27
2.4.1. Metallographic preparation of sprayed coatings	27
2.4.2. Scanning electron microscope (SEM) analysis	28
2.5. Experimental procedure of ex situ coating property (ECP) sensor.....	29
2.5.1. Specimen preparation.....	29
2.5.2. Coating thickness measurement	29
2.5.3. Bilayer curvature-temperature (BCT) measurements	30
2.5.4. Anelasticity parameters function.....	35
3. Results and discussion	36
3.1. Suspension plasma sprayed YSZ coatings microstructure	38
3.1.1. Effect of torch raster speed (LS).....	39
3.1.2. Effect of torch-substrate distance (stand-off distance) (HD)	40
3.1.3. Effect of plasma gas composition (GC)	41

3.1.4.	Effect of current and plasma power (HP).....	42
3.1.5.	Effect of internal nozzle diameter (ID).....	43
3.2.	Design of experiments for ex-situ coating property (ECP) process.....	44
3.3.	Anelastic parameters and curvature-temperature responses	45
3.3.1.	High power (HP)	46
3.3.2.	High stand-off distance (HD)	48
3.3.3.	Low raster speed (LS).....	50
3.4.	Sensitivity of curvature-temperature responses to the spraying conditions.....	51
3.5.	Anelastic parameters of coatings and their corresponding microstructure	51
3.6.	Evaluation of elastic modulus of SPS YSZ coatings	58
4.	Conclusion and future work.....	59
References	63

List of Figures

Figure 1-1. Diagram of the thermal spray coating process showing the spray torch, high-energy gas stream with coating material and substrate with deposited coating [3].	2
Figure 1-2. Schematic of a plasma spray process showing the various components of the system [5].	2
Figure 1-3. Schematic of a suspension plasma spray process [14].	4
Figure 1-4. Droplet fragmentation and evaporation model proposed by Wittman /Fazilleau [15].	4
Figure 1-5. Transverse fracture surface of a standard air plasma spray APS (Left) coating and a suspension plasma spray SPS (Right) coating [23].	7
Figure 1-6. Schematic of coating microstructure change with decreased particle size[25].	8
Figure 1-7. The main features of fractured cross section of YSZ manufactured by SPS [23].	9
Figure 1-8 .Stress vs. strain curves determined for plasma-sprayed ZrO_2 -8wt% Y_2O_3 thermal barrier coatings: (a) uniaxial tension; (b) compression; (c) biaxial flexure; (d) uniaxial flexure showing responses of tension and compression sides. The numbers of loading unloading cycles are indicated at the top of the curves from (a) to (c). T is tension; C is compression in (d)[44].	11
Figure 1-9. Anelastic behavior determined for 8wt% Y_2O_3 - ZrO_2 : a) In-situ SEM observation of interfaces displacement; (b) Cyclic stress-strain curve exhibited both non-linearity and hysteretic responses [47].	11
Figure 1-10. Stress-strain relation showing nonlinearity and hysteresis during thermal cycling of plasma sprayed (YSZ) coating [51].	12
Figure 1-11. Schematic description of mechanisms responsible for anelastic behavior of ceramic coating [50].	13
Figure 1-12. Schematic of curvature change as coating and substrate is thermal cycled. Coating and substrate impose equal and opposite forces on each other and create unbalanced moment. The bending moment is balanced by a curvature of the coating/substrate composite [60].	14

Figure 1-13. Schematic of curvature - temperature measurement device, ex situ coating property (ECP) [64].	15
Figure 1-14. Anelastic behavior of plasma sprayed YSZ on Al substrate. a) Nonlinearity and hysteresis of curvature-temperature plot when subjected to thermal loading [66]. b) Nonlinearity and hysteresis in stress-strain relationship, and also key parameters of anelastic behavior[50].	16
Figure 2-1. Substrate preparation steps. a) stainless-steel before cleaning and grit blasting. b) Aluminium oxide (Al_2O_3) for grit blasting with particle size of $\sim 200 \mu m$. c) Substrate (stainless-steel) after cleaning and grit blasting. d) Substrate roughness measurement with 3D laser microscope.	19
Figure 2-2. Suspension preparation contents and formulation.	20
Figure 2-3. Suspension characteristics. a) Particle size distribution through laser light scattering technique, showed average particle diameter $D_v(50)=0.385(\mu m)$. b) Suspension viscosity measurement result by automatic rheometer instrument provided a dynamic viscosity of 5.25 (mpa-s).	21
Figure 2-4. Schematic description of suspension feeding system.	23
Figure 2-5. Schematic description of torch raster pattern. a) Representation of the plasma torch with different temperature regions scanned over a flat surface and bead overlapping formation mechanism. b) Spray pattern for one coating pass used in this study.	25
Figure 2-6 Substrate and sample holder with thermocouple. a) Front view. b) Top view	29
Figure 2-7. Coating thickness measurement under optical microscope	30
Figure 2-8. The photograph and schematics of ECP device which is thermal cycling the beam through using a muffle furnace. Measure the temperature and curvature of the specimen using welded thermocouple and three laser displacement sensors, respectively.	31
Figure 2-9. A repeatable curvature-temperature plots obtained from heating and cooling both in the furnace for one sample. First cycle (1h) is different from the consecutive cycles. Also in this specimen during fifth cycle (5h) in the heating part, foreign media decrease the lasers intensity, and interfere the data points in a region.	32
Figure 2-10. Initial steps to quantify the anelastic properties of YSZ coatings. The selected repeatable curvature-temperature response which is qualified for further analysis. The heating curve of thermal cycle is plotted separately to determine the temperature range over	

which the thermal cycle was performed, and to select the transition point in which the curve started its nonlinear behavior.....	33
Figure 2-11. A typical curvature-temperature plot obtained from ECP measurements for a SPS YSZ coating. Hysteresis behavior between heating and cooling cycle, and related parameters to calculate hysteresis degree.....	34
Figure 3-1 SEM pictures of six SPS YSZ coatings microstructure deposited under different spraying parameters. A) T1 (Ref). B) T2 (LS). C) T3 (HD). D) T4 (GC). E) T5 (HP). F) T6 (ID).	37
Figure 3-2. SEM pictures of SPS YSZ coating microstructure produced at T1 (Ref) condition. A) Low magnification with (a) segmentation cracks and columnar feature. B) High magnification with (b) dense regions of YSZ deposited (c) porosities (d) overspray regions of YSZ coating with very fine pores.	38
Figure 3-3. SEM pictures of SPS YSZ coating microstructure produced at low raster speed (LS) condition. A) Low magnification with (a) segmentation crack and inter-pass boundaries. B) High magnification with (b) dense regions of YSZ deposited (c) porosities (d) overspray regions of YSZ coating with very fine pores are labeled.....	39
Figure 3-4. SEM pictures of SPS YSZ coating microstructure produced with high stand-off distance at (HD) condition. A) Low magnification with high density of overspray particles formed YSZ coating very fine pores. B) High magnification with (d) overspray regions of YSZ coating with very fine pores, and (e) re-solidified particles in the spheroid form embedded in the coating structure marked by red circles.....	40
Figure 3-5. SEM pictures of SPS YSZ coating microstructure produced with Ar/H ₂ plasma gas composition at (GC) condition. A) Low magnification with (a) segmentation crack started to initiate due to temperature gradient. B) High magnification with (b) dense regions and (d) overspray regions of YSZ coating with very fine pores.....	41
Figure 3-6. SEM pictures of SPS YSZ coating microstructure produced with high power at (HP) condition. A) Low magnification with (a) segmentation crack. B) High magnification with (b) dense regions of YSZ deposited (c) porosities (d) overspray regions of YSZ coating with very fine pores.....	42
Figure 3-7 SEM pictures of SPS YSZ coating microstructure produced with larger internal nozzle diameter at (ID) condition. A) Low magnification with (a) segmentation crack. B)	

High magnification with (b) dense regions of YSZ deposited (c) porosities and (f) oblique crack due to poor bonding strength between layers in two consecutive passes.	43
Figure 3-8. Three different SEM pictures of SPS YSZ coating microstructure. A) Lower raster speed (LS) with inter-pass boundaries structure. B) High stand-off distance (HD) with considerable porous regions. C) High power (HP) with denser region than (LS) condition comprising segmentation cracks within its structure.	44
Figure 3-9. Substrate temperature measurement for different spraying parameters through attaching the thermocouple on the back side of the substrate.	45
Figure 3-10. Coating thickness measurement for different samples (HP-A, HP-B, HD-C, HD-D, LS-E, and LS-F). The central parts are thicker than the edges in all samples due to higher overlapping density in the central zone.	46
Figure 3-11 Curvature-temperature responses of SPS YSZ at high power (HP) condition. A) Second (2h) and third (3h) cycle of sample A, and B) Second (2h) and third (3h) cycle of sample B are qualified for analysis.	47
Figure 3-12. Calculation of hysteresis degree (HD). A) Second thermal cycle (2h) of sample A disregarding the hysteresis pattern of regular plasma spray, and B) second thermal cycle (2h) of sample B following the hysteresis pattern of regular plasma spray.	48
Figure 3-13. Curvature-temperature responses of SPS YSZ at high stand-off distance (HD) condition. A) Second (2h) and third (3h) cycle of sample C, and B) second (2h), third (3h) and fourth (4h) cycle of sample D are qualified for analysis.	49
Figure 3-14. Curvature-temperature responses of SPS YSZ at low raster speed (LS) condition. A) Second (2h) third (3h), fourth (4h), and sixth (6h) cycle of sample E, and B) second (2h), third (3h), fourth (4h) and seventh (7h) cycle of sample F are qualified for analysis.	50
Figure 3-15. Curvature-temperature sensitivity to spraying condition. The second cycle (2h) of all samples is selected to illustrate the sensitivity of curvature changes to the spraying condition under constant thermal strain ($\Delta\varepsilon = \Delta\alpha \times \Delta t$) for all samples.	51
Figure 3-16. Map of non-linear elastic properties of SPS YSZ coatings to distinguish properties of various specimens manufactured in different spraying condition.	52

Figure 3-17. SEM pictures of six SPS YSZ coatings microstructure. A) and B) produced under high power condition (HP). C) and D) coated under high stand-off distance (HD) condition. E) and F) deposited under low raster speed (LS) condition.....	53
Figure 3-18. Coating deposition pattern, and the influence of plasma torch raster speed on the thickness of dense and porous zone of deposited bead.....	55
Figure 3-19. SEM pictures of SPS YSZ coating microstructure. A) Before thermal cycling with inter-pass boundaries. B) And C) after thermal cycling.....	56
Figure 3-20. Map of elastic modulus (E) and secant modulus (E_{sec}) to distinguish the coatings compliance and flexibility.....	57

List of Tables

Table 2-1. Summary of suspension properties measurement	21
Table 2-2. Main characteristic of 3MB plasma gun.....	22
Table 2-3. Process parameters of suspension plasma spray	26
Table 2-4. Grinding and polishing steps with specific parameters	28
Table 3-1. Anealstic parameters of SPS YSZ in high power (HP) condition.	47
Table 3-2. Anealstic parameters of SPS YSZ in high stand-off distance (HD) condition. ...	49
Table 3-3. Anealstic parameters of SPS YSZ in low raster speed (LS) condition.	50
Table 3-4. Evaluation of elastic modulus of SPS YSZ coatings	58

1. Introduction and literature review

Over many years, coating technologies on the industrial parts (aerospace, transportation, petrochemical, electronics and medical applications) with a different material have been used extensively to create engineered surfaces. To improve functional performance and extend the component life which is working under corrosion/erosion environment or thermal/mechanical shock, and also to restore worn or poorly machined parts to the original dimensions and specifications, can be considered as the main goals to for the coating industry[1].

In general, coating technologies can be categorized into **thin** - and **thick** - film technologies. **Thin films**, with the thickness of less than a hundred micron can be produced by dry coating processes like chemical vapor deposition (CVD) or physical vapor deposition (PVD). They offer excellent enhancement of surface properties by using small quantities of raw materials. However, limitation on the size and shape of the substrate, slow application process and low deposition rate, and also requirement of reduced pressure environment add more complication on these types of coating processes. On the other hand, **thick** films have a thickness from a hundred micron, up to several millimeters. Coating thickness depends on required performance, and environmental condition. Thick film deposition methods include chemical/electrochemical plating, brazing, weld overlays, and thermal spray[1,2].

“Thermal spraying comprises a group of coating processes in which finely divided metallic or nonmetallic materials are deposited in a molten or semi-molten condition to form a coating. The coating material may be in the form of powder, ceramic rod, wire, or molten materials”[3].

High deposition rate, low operating cost, and flexibility with a broad range of material selections and capability of coating deposition on complex geometries persuade the surface engineering society to develop the thermal spray technology. In general, all thermal spray processes include: **I.)** Spray torch supplied by gas and power which convert chemical or electrical energy to thermal and kinetic energy to melt and accelerate the particles respectively **II.)** The injection of material into the high-energy gas stream, and its transformation into a stream of molten droplets **III.)** Molten and accelerated particles impact to the prepared substrate and solidify rapidly forming individual “splats” that are building blocks of layered coatings (see Fig 1.1)[3].

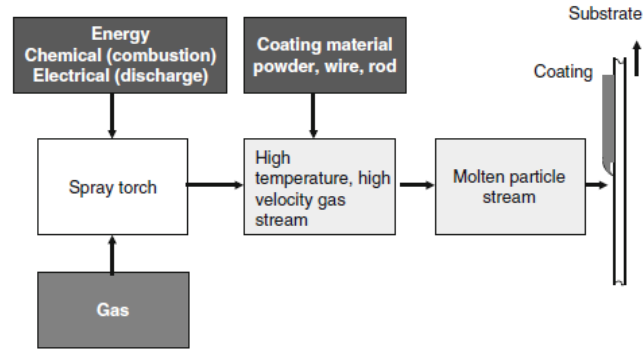


Figure 1-1. Diagram of the thermal spray coating process showing the spray torch, high-energy gas stream with coating material and substrate with deposited coating [3].

Plasma spraying is a subset of thermal spray processing, in which metallic and non-metallic materials in the form of powder are deposited in a molten or semi-molten state on a prepared substrate[4]. In plasma spraying, the heat source is generated by an electric arc within a plasma torch consisting of a cathode and anode (made of tungsten and copper, respectively) and through introducing the argon or nitrogen gas with also helium or hydrogen as a secondary gas to increase the enthalpy of the plasma gas[5]. The plasma gas exits the nozzle as a high-temperature, high-velocity jet, which melts and accelerates the powder carried by an inert gas such as Ar (see Fig. 1.2). These molten and semi-molten particles propel toward the substrate, then undergo rapid solidification on the substrate surface resulting in making a lamellar structure by the layering of splats.

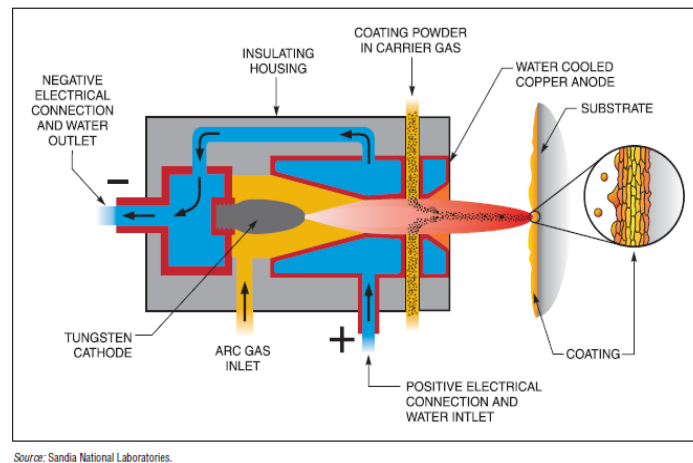


Figure 1-2. Schematic of a plasma spray process showing the various components of the system [5].

Coatings properties can be characterized by investigation on splats shape, size and also quality of inter-bonding/interfaces between them[6]. Since the microstructure of coatings is very sensitive to the feedstock particle size, the importance of developing and studying submicron structure with significant improvement in engineering properties can be addressed due to the following reasons:

I.) Reduction of grain sizes (high cooling rate) by a factor of almost two orders of magnitude over conventional coatings resulted in increasing strength, improving toughness and hardness which provide better wear and thermal shock resistance [6].

II.) The large volume fraction of internal interfaces (thinner splats) increases the coating's resilience and mechanical compliance at high operating temperature which can result in better resistance to thermal mismatch strain [7–9].

III.) High boundary defects density, and finer pores decrease the phonon mean free path cause lower thermal diffusivity/conductivity for ceramics in thermal barrier coating applications [8,9].

IV.) Better cohesion between splats with sizes in a few hundred nanometers leading to higher compliance response and stain tolerance with the substrate, especially in the aircraft and land-based turbine engines industry working in high operating temperature [10,11].

Decreasing the average particle size down to the submicron-scale brings up some technological issues. To inject submicron particles with low momentum and inertia into the core of high enthalpy plasma gas flow, the particle injection momentum and force should be higher than that one applied in the conventional plasma spray. However, increasing of cold carrier gas flow rate (over 1/5 of that of forming the plasma gas) disrupts the plasma jet, and decreases the deposition efficiency[12]. In addition, using conventional plasma spray injection equipment to feed these submicron-scale particles into the plasma plume could result in blocking of the injection line, since they tend to form larger aggregates during spraying due to dominant electrostatic surface forces [13]. To circumvent these drawbacks, the injection of such particles into a plasma jet with high efficiency can be achieved with the help of a liquid carrier as a suspension made by submicron ceramic particles, and ethanol or water as a solvent, and also dispersant to prevent particles from agglomeration.

1.1. Suspension Plasma Spray process

Suspension plasma spraying (SPS) is a novel method of plasma spraying process using submicron particles dispersed in a liquid (ethanol or water typically) to inject them directly into the plasma plume (See Fig. 1.3). In SPS, the suspension is injected into a direct current (D.C.) plasma jet at atmospheric pressure by using a pressurized container in which the liquid is stored and forced through a nozzle [14]. Upon penetration, the plasma-liquid interaction fragments the suspension into smaller liquid droplets by aerodynamic drag forces from the plasma flow (See Fig. 1.4). Once the fragmentation of the suspension has happened, solvent begins to evaporate (two orders of magnitude longer than fragmentation) and lead to agglomeration and melting the solid content exposed to the large temperatures of the plasma jet. Molten particles then accelerate toward the preheated substrate where they flatten and solidify to form splats and the coating structure [15].

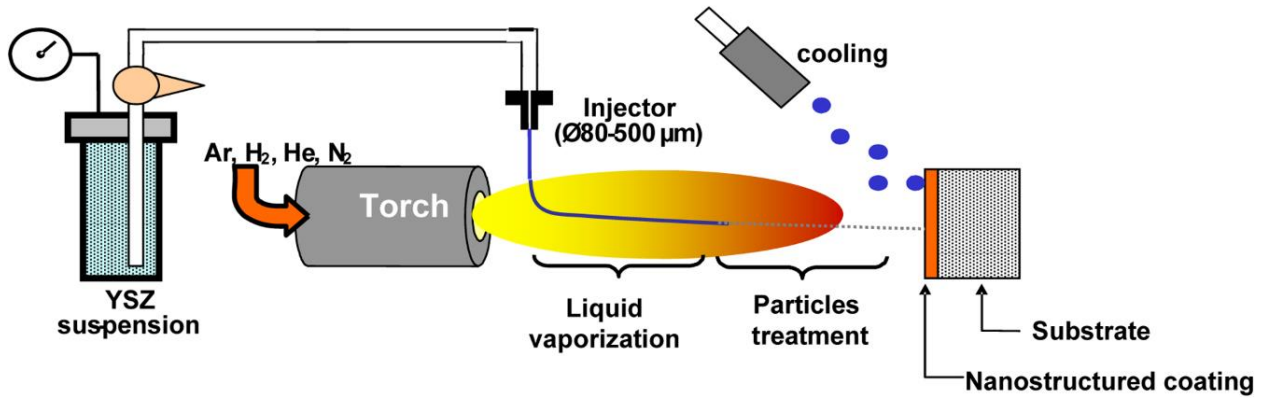


Figure 1-3. Schematic of a suspension plasma spray process [14].

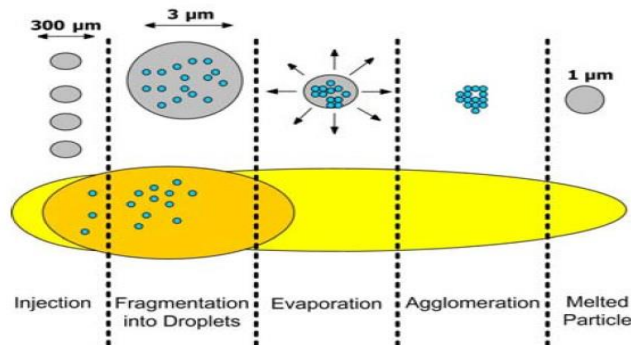


Figure 1-4. Droplet fragmentation and evaporation model proposed by Wittman /Fazilleau [15].

Compared to conventional plasma spraying, SPS is by far more complex regarding the reproducibility of spraying process and coatings properties for the following reasons:

- The injection of suspension into the plasma plume has to be controlled to meet the required condition for the continuous liquid stream and more homogeneous treatment of the suspension within the plasma jet, meaning that the momentum density of the liquid droplets has to be higher than the momentum density of the plasma flow. For the ones with lower momentums, they will very likely travel at the fringes of the flow where the solvent will be evaporated but the droplet contents will be poorly melted, thus impacting the substrate in a semi-molten state, and increasing the porosity of the deposit if they stick to it [16].
- The thermal and kinetic inertia of hot particles are very low which means that the heating and cooling rates of particles are very rapid, and they also decelerate faster than bigger ones, then requiring SPS uses shorter standoff distances between the plasma torch exit and the substrate than conventional plasma spraying. So, the plasma jet imposes a very strong heat flux to the coating/substrate during deposition and it could result in a coating densification and reducing porosity [17].
- Arc root fluctuations have an important influence on plasma instabilities and shear force which is breaking up the suspension into finer droplets. In SPS, this influence is more pronounced since the fluctuations act on jet penetration, fragmentation, particle trajectories, heating and acceleration. Large arc fluctuation increases the inhomogeneity of fragmentation/vaporization within the plasma flow and dispersion angle which leads to disturbing the transferring of thermal and kinetic energy to the droplets and particles [16,18,19].
- Suspension preparation is considered as one of the most important factors in SPS process. It should be underlined that suspension must be stable, maintaining good particle dispersion (without agglomeration) to prevent the injector from clogging, and also have a narrow particles size distribution to achieve more homogenous coating architecture. Narrow particle size distribution decreases the inhomogeneous thermal treatment of particles, thus promoting dense coatings, whereas suspension with broad particle size distribution reduces the uniform behavior of the liquid droplets stream, and trajectory of solid particles, therefore they tend to form porous coatings [12,17].

1.2. Improved microstructure of thermal barrier coating (TBC) provided by submicron particles

Thermal barrier coatings (TBC) protect metallic components of the hot sections of aerospace, and land-based gas turbines working at high operating temperature (up to 1450°C) from degradation and failure. Thermal conductivity is one of the main material properties of the coating to insulate the underlying superalloy structure. Although any material specially ceramics with a low thermal conductivity can be used as a TBC, yttria-stabilized zirconia (YSZ) has been chosen and accepted by industry standards due to its lower thermal conductivity and much more stabilized phase (thanks to Yittria (Y_2O_3)) than other ceramics at elevated temperature. A relatively low elastic modulus of plasma sprayed YSZ enables it to be more resilient under some deformation without brittle fracture. Also higher thermal expansion coefficient of YSZ ($10 \mu\text{m/m}^\circ\text{C}$) than other ceramics permits the coating to be more compatible with the substrate in terms of thermal mismatch strain and shrinkage rate from the time the spraying ends until both coating and substrate come to an equilibrium temperature, thereby preventing coating from delamination [20, 21].

Thermal-barrier coatings are traditionally made either by air plasma spray (APS) or electron-beam physical vapor deposition (EB-PVD) process. Due to the differences in the coating deposition principle both these techniques produce distinctively different coating architectures. In fact, the EB-PVD process offers better coating mechanical properties and durability than APS because of its columnar structure that can tolerate larger amounts of strain. However, higher deposition rate, and process flexibility, and also more cost effective of plasma spray than EB-PVD promote to develop and manufacture TBC coatings by plasma spray process with improved microstructure and mechanical properties [20–22].

Compare to APS ceramic coating, SPS allows achieving finely structured layers formed by thinner splats, therefor SPS ceramic coating offers an increased number of lamellas (See Fig. 1.5). Suspension plasma spraying of yttria stabilized zirconia (YSZ) coatings have demonstrated a number of desired properties when compared to air plasma spray (APS) or electron beam-physical vapor deposition (EB-PVD) coatings. The SPS process has the potential to generate coatings with increased density of lamellas interfaces than APS coatings which enables the ceramic lattice to impede and disrupt the phonons path and IR radiation through the coating structure, then decreasing the thermal conductivity of ceramic layers more than what is common in APS coatings[22].

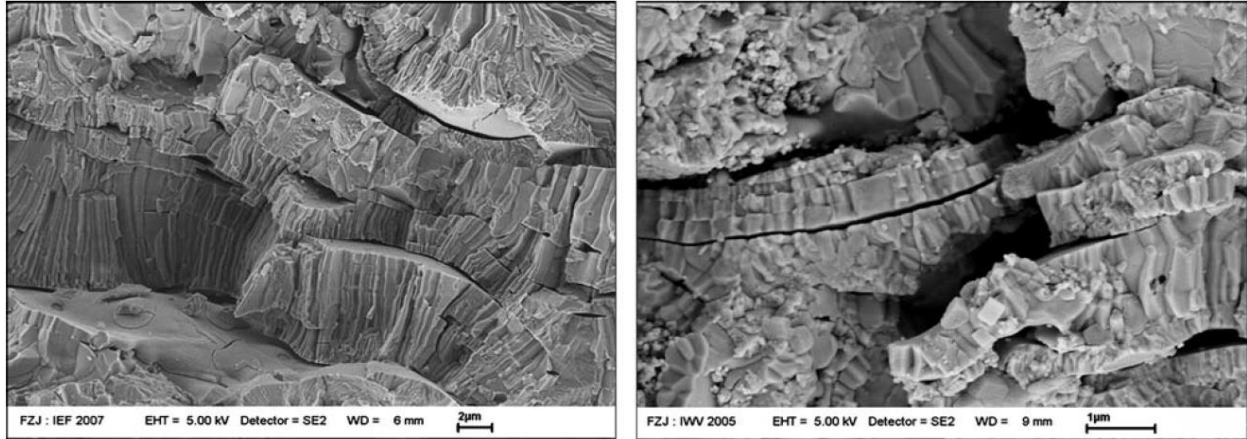


Figure 1-5. Transverse fracture surface of a standard air plasma spray APS (Left) coating and a suspension plasma spray SPS (Right) coating [23].

The SPS process allows the production of coatings with a columnar structure to provide the strain tolerant behavior of EB-PVD, but with the higher volume of fine pores. The mechanism for generation of the coating columnar structure can be related to the influence of plasma drag force on the trajectory of small in-flight particles and angle of impact. Particles in submicron-scale have relatively low momentum, so strong influence of plasma flow redirect the particles trajectory from normal to along direction of the substrate surface to impact at a shallow angle on the substrate asperities resulting in coating builds-up in columnar structure (See Fig. 1.6). It has been investigated, when the substrate surface roughness was higher than the average diameter of the feedstock particle the chance of shallow impact angle increases which can be led to the formation of columnar structures in the deposited coating. Control of columnar microstructures is dependent on the size of the droplet generated during the atomization and the size of the impacting particle, and also the substrate surface roughness [12, 24, 25].

The formation of segmented structure in SPS process can also be explained by the tensile stress (quenching stress) emerging from temperature gradient between molten particles and preheated substrate. In fact, quenching of molten particles is restricted by underlying substrate or previously deposited layer. Tensile stress can be relaxed by micro-cracks formed during energy release of splat cooling resulting in segmentation crack formation. Suspension plasma spray of submicron particles could also offer coating structure with segmentation cracks and higher volume of fine pores which increases strain tolerant and decreases thermal conductivity [26].

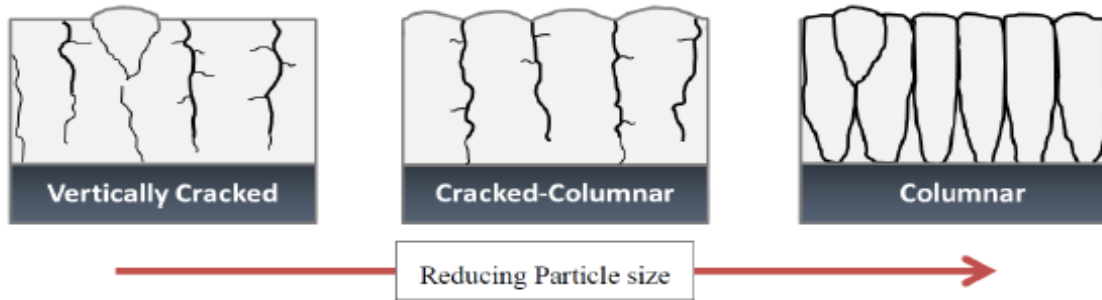


Figure 1-6. Schematic of coating microstructure change with decreased particle size[25].

It is well known that when TBCs are exposed to high operating temperature for extended periods of time, sintering takes place within the coating structure, and it may have an effect on reducing the coating strain tolerance and promoting failure in thermal cycling operations. Due to the nature of SPS process, the manufacture of submicrometer-structured coating offers the presence of areas includes the dense and porous nano zones with different sintering rate [27]. It has also been reported that the retention of embedded porous nano zones provided by submicron particles exhibited faster shrinkage rate than the dense zones due to higher surface area resulted in the opening of large micron-sized voids in the coating structure and reduction of sintering and elastic modulus increasing rate [28]. In fact, the large fraction of very fine pores in the coating structured manufactured by submicron particles induce a high specific surface area and retard the sintering effect.

1.3. Microstructural features of suspension plasma sprayed TBCs

Since thermal barrier (TBC) coatings expose to the high heat flux in a combustion environment, predicting the service life of these coatings and their reliability should be considered as a critical issue. The degradation and failure of the thermo-mechanical properties of the TBC coating are related to different phenomena which arise within its microstructure. For evaluation of coatings performance and durability, it is necessary to take into consideration the unique and novel microstructure of TBCs coating manufactured by suspension plasma spray (SPS). Due to the liquid injection of the small size of the powdery feedstock, and also fragmentation, vaporization of droplets, SPS offers to attain specific microstructural features. (See Fig. 1.7)

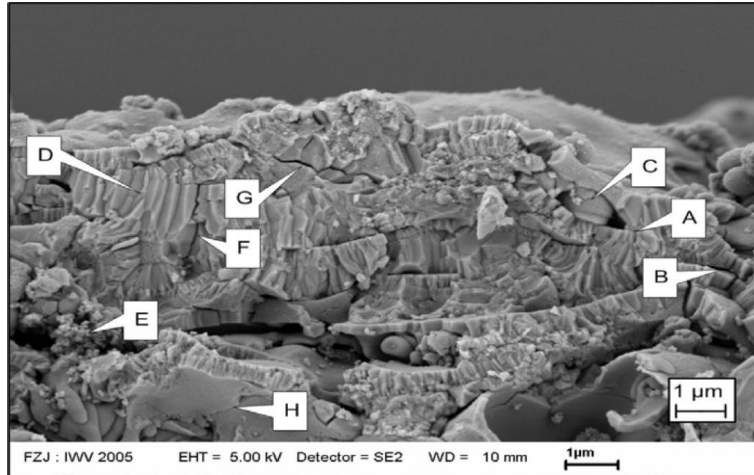


Figure 1-7. The main features of fractured cross section of YSZ manufactured by SPS [23].

Based on the flattening degree of splats which depends on the dynamic and heat treatment of solid particles within the plasma jet, areas of perfect (A) and incomplete (B) inter-splat bonding can be deposited in the coating structure[15, 29]. In-flight particles in semi-molten or partially molten (unmolten inner core) state might be re-solidified (C) due to long distance condition between the torch and the substrate (high stand-off distance) [12, 19]. The high cooling rate of small molten particles (thinner splat) leads to high nucleation rate with small crystal sizes to form polycrystalline lamellae. Crystals grow rapidly opposite to the direction of heat flux to form and building-up columnar grains (D) in the structure of the coating [30]. Clusters of unmolten/semi-molten particles, known as “overspray,” (E) can be deposited ahead of and behind the fully molten particles on the substrate when torch passes over the substrate [31]. The segmentation cracks (F) initiate and propagate during the deposition phase due to stress relaxation. Particle solidification is hindered by underlying substrate or previously deposited layers making in-plane tensile stress within splat which can be relaxed through the initiation of micro-cracks within the splat. The good inter-splat/inter-layer bonding enables crack to propagate from one splat to another [32, 33]. Low substrate and particle temperature might be led to decreasing the bonding strength between lamella with the low contact area, and also high tensile stress from recently molten particles can result in a generation of (G) horizontal crack [32, 33]. Microcrack network on an individual splat (H) can be explained by the energy release of splat during cooling as a consequence of the relaxation of the quenching stress (tensile stress) [34, 35].

The nature and morphology of coatings microstructure provided by suspension plasma spray have an effective influence on the mechanical and thermal characteristic of coatings [36,37]. Moreover, the inhomogeneous structure and anisotropic behavior of ceramic coating's properties will add more complexity to evaluate their performance under different thermal and mechanical loading [35, 38].

The coating's properties, such as stress-strain relation, thermal conductivity [36] and residual stresses [39] are very dependent on size, shape and level of porosity and micro-cracks which are inherently embedded in the coating's structure. These defects are the main reasons for the SPS coatings to have more distinct properties than that of bulk material. Understanding the role of the defects and their mechanism can provide sufficient judgment into the coating properties.

1.4. Anelastic behavior in plasma sprayed ceramic coating

Plasma sprayed ceramic coating properties are dependent on the defect architecture, and their behavior while experiencing a significant amount of stress changes in the gas turbine engine. In order to understand the mechanisms governing stress-strain relation in ceramic coatings, an advanced perception of the microstructure, and its correlation to applied load is required.

1.4.1. Background

An inhomogeneous and anisotropic microstructure of plasma sprayed ceramic coatings dominate the physical and functional properties of the coatings. The properties of coatings are very sensitive to the defect architecture, special lamellar structure, and presence of discontinuities like pores, microcracks and splat boundaries. This also explains why the elastic properties of thermal sprayed coatings are significantly different from those measured in the same bulk materials processed by other means, and may vary with the spray conditions employed for deposition.

Many works have also shown that plasma sprayed ceramic coatings have no linear behavior in their stress-strain system and elastic modulus under different mechanical loading [40–48]. For example in one experiment which was done by Sung R. Choi and his colleges, the free-standing (without substrate) YSZ coatings were tested under different modes of load-unload cycles comprising uniaxial tension, compression, and flexure (four and three-point bending test) (See Fig. 1.8) [44]. Results proved that tested coatings had not only non-linear behavior but also exhibited hysteretic response in their stress-strain curve, collectively named as anelastic behavior of the coating. They also observed the mechanical behavior of coating is time-dependent meaning that

by increasing the tensile and compressive load, coatings modulus and stiffness decreased and increased, respectively.

In the investigation of previous works, the anelastic behavior of plasma sprayed ceramic coating was attributed to their lamellar features and coating's microstructure [40–48](See Fig.1.9). For instance, through in-situ SEM observation, the relative sliding or movement of defects under tensile loading was shown to introduce the anelasticity in stress-strain curve of the YSZ coating.

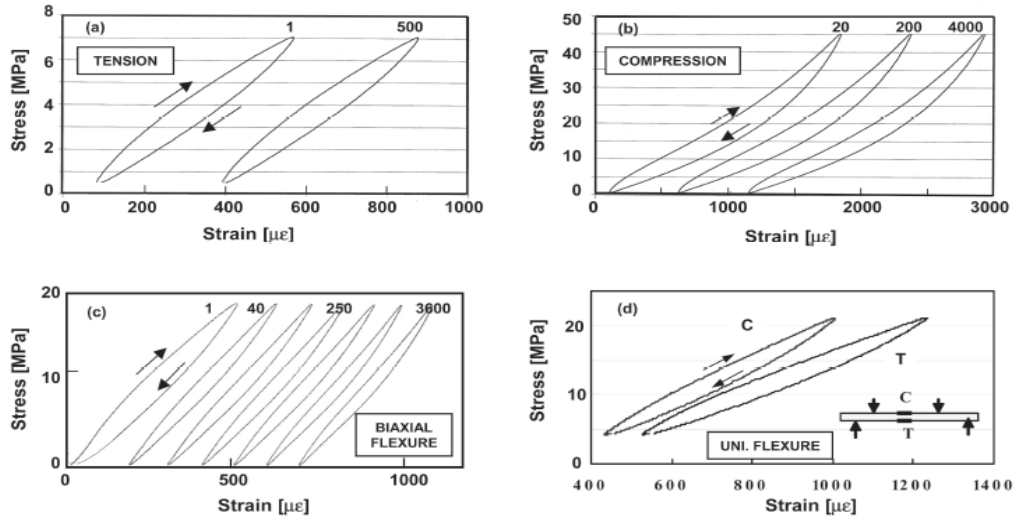


Figure 1-8 .Stress vs. strain curves determined for plasma-sprayed ZrO₂-8wt% Y₂O₃ thermal barrier coatings: (a) uniaxial tension; (b) compression; (c) biaxial flexure; (d) uniaxial flexure showing responses of tension and compression sides. The numbers of loading unloading cycles are indicated at the top of the curves from (a) to (c). T is tension; C is compression in (d)[44].

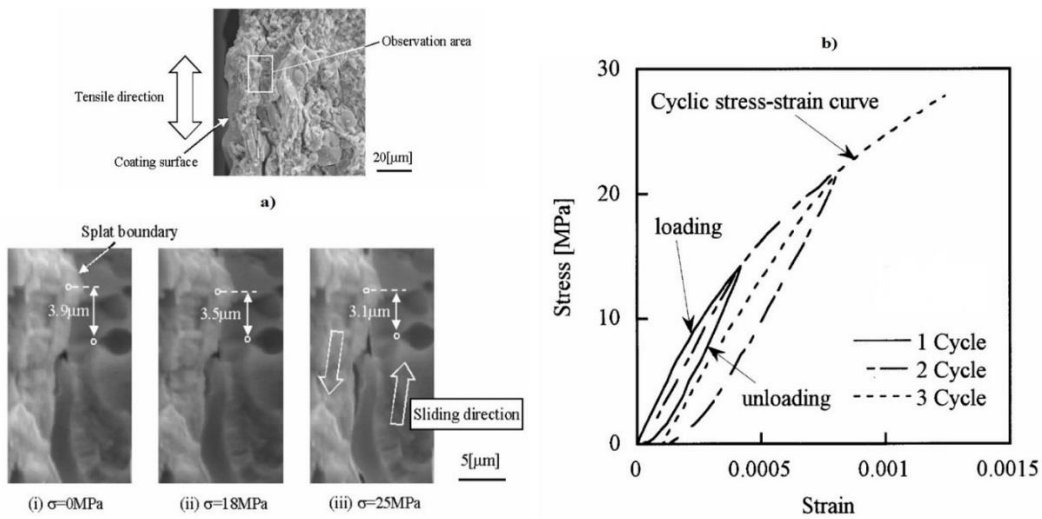


Figure 1-9. Anelastic behavior determined for 8wt% Y₂O₃ - ZrO₂: (a) In-situ SEM observation of interfaces displacement; (b) Cyclic stress-strain curve exhibited both non-linearity and hysteretic responses [47].

Plasma sprayed YSZ also showed the anelastic behavior under thermal loading through curvature-temperature method [49–51]. It was investigated that the coating-substrate bi-layer system is non-linear as well as hysteretic under thermal loading (See Fig. 1.10). To evaluate the thermal mismatch stresses between the coating and the substrate under temperature change, YSZ deposited on an aluminum substrate. In their experiment, the coated specimen was heated by using a flame torch or a box heater generating thermal mismatch stresses (tensile stress) on the coating. Once the system reached the maximum tensile stress, it was cooled to the onset temperature and the system returned to its initial stress state. The coating showed the non-linearity behavior during both the heating and cooling phases, and the stress-strain curve exhibited hysteresis in it, same as what was seen from previous works when the mechanical loading was applied.

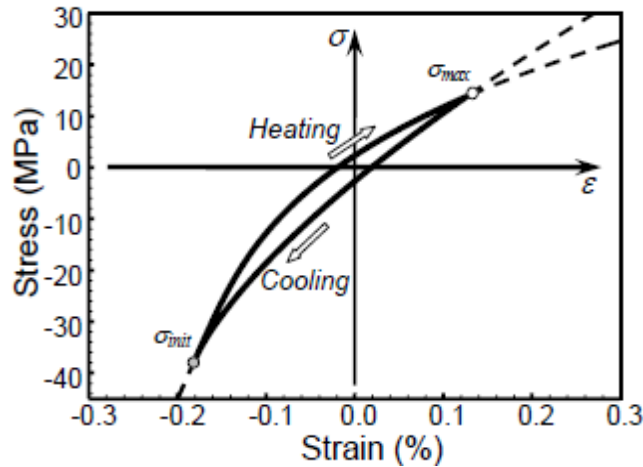


Figure 1-10. Stress-strain relation showing nonlinearity and hysteresis during thermal cycling of plasma sprayed (YSZ) coating [51].

The proposed mechanism behind the anelastic behavior of PS YSZ coating under thermal loading was correlated to displacement of defects within coating structure [50](See Fig. 1.11). It was suggested that the source of nonlinearity originates from the opening/ closure of micro-cracks and pores at elevated temperature. In fact, at room temperature, the cracks faces are closed, and the coating exhibits higher apparent stiffness than in higher temperature when tensile stresses induce the cracks and pores to open. Also, it was proposed that the hysteresis behavior in a complete loading-unloading cycle of thermally sprayed ceramic coating is correlated to the produced frictional sliding and corresponding energy dissipation within the interfaces at coating's lamellar structure.

The results of all mentioned previous works confirmed that the plasma sprayed ceramic coatings have anelastic behavior in their stress-strain curve due to their unique architecture of microstructure.

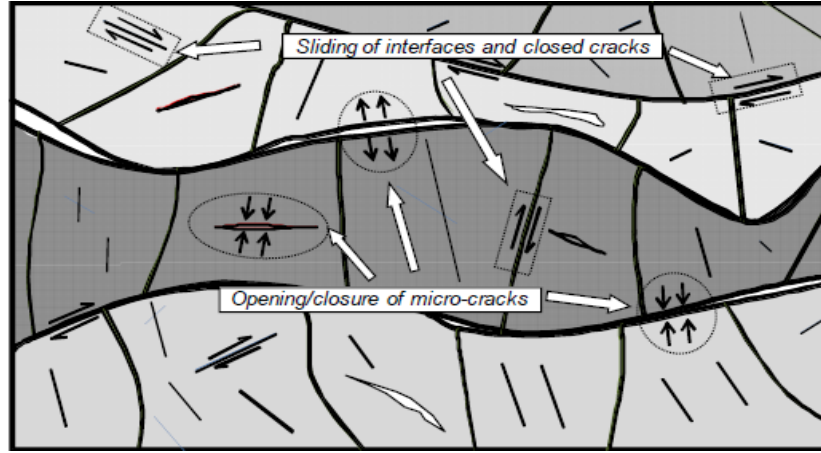


Figure 1-11. Schematic description of mechanisms responsible for anelastic behavior of ceramic coating [50].

1.5. Evaluation of anelastic behavior of plasma sprayed ceramic coating through Bi-layer Curvature-temperature (BCT) method

Thermal barrier coatings (TBCs) applied to the blades in gas turbine engines are exposed to thermal and mechanical stresses due to thermal mismatch at high operating temperature, and the motion of blades, respectively. Thereby, evaluation of coating's mechanical properties regarding modulus and stress-strain relationship should be considered as important criteria for the performance efficiency and longevity of the coatings. The elastic modulus as a coating's mechanical property which depends on the defect architecture is an indicator of coating integrity, bonding quality between lamella, and also its stiffness. It should be noted that higher elastic modulus at low strain provides greater durability resistance for coatings. However, at high operating temperature the low elastic modulus and increased flexibility of TBC coating is required to meet the thermal mismatch strain. As discussed earlier, plasma sprayed ceramic coatings contain numerous defects (pores, cracks) which have a significant influence on the elastic modulus, and also non-linearity behavior of stress-strain relationship.

Bi-layer curvature-temperature (BCT) method is an efficient procedure to estimate the modulus of coating at low strain (initial stiffness), and also at the elevated temperature which is related to its degree of defects movement within coating structure. The curvature measurement to determine

properties of thin films on thick substrate was introduced by Stoney (1909) [52]. Mechanical properties of thin film produced by plasma-enhanced chemical vapor deposition (PECVD) [53], RF magnetron sputtering [54–56], plasma-based ion implantation [57] and electroplating [58], were investigated based on Stoney formula. It should be underlined, in all previous works, the coating thickness was less than 1 μm . The limitation of stony formula is that the thickness of coating must be relatively small as compared to that of the substrate. For coatings that are thick, curvature solutions must be obtained with an alternate method. A robust procedure to measure and quantify the nonlinear mechanical properties of the thick thermal sprayed ceramic coatings based on curvature-temperature measurement has been proposed by Nakamura and his colleagues [49,59,60]. In their experiments, thermal cycle tests were performed with a heater box or a gas torch gun moved across YSZ coating surface to heat specimen until specific maximum temperature. In fact, in temperature excursions, the coating-substrate system experiences thermal mismatch stresses due to the difference in coefficient of thermal expansion (CTE) resulting in a change in curvature of the bi-layer assembly. (See Fig. 1.12). In general, the CTE of ceramic coating is less than that of metallic substrates, then during heating, the coating is under tensile stress, while during cooling down coating tends to be more compressive.

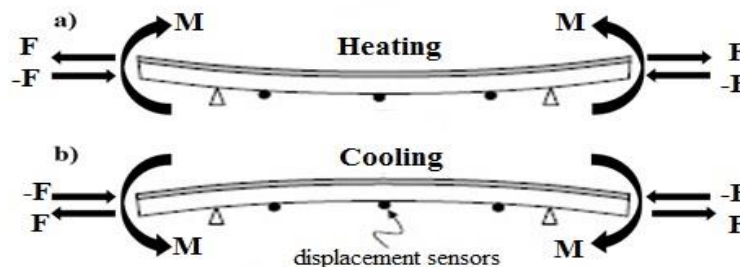


Figure 1-12. Schematic of curvature change as coating and substrate is thermal cycled. Coating and substrate impose equal and opposite forces on each other and create unbalanced moment. The bending moment is balanced by a curvature of the coating/substrate composite [60].

For precise extraction of the radius of curvature, three laser displacement sensors with perpendicular measurement axis were placed on the back of the substrate. Also, the temperature variation was recorded through using thermocouple attached to the substrate. The measured curvature-temperature data was processed, then through inverse analyses method the stress-strain relation of a coating could be calculated [59]. It should be noted, the inhomogeneous thermal gradients and uneven isothermal conditions in the thermal cycle (heating and cooling) performed

with the flame torch and heater box methods resulted to large fluctuations in curvature measurements[50].

A recently developed substrate curvature measurement device, ex-situ coating property (ECP) sensor, which is based on the principle of previous works has been applied to quantify the coating's anelastic behavior under controlled temperature changes[50,61–64]. (See Fig. 1.13). In ECP test procedure a coated substrate is mounted inside a muffle furnace to provide more controlled and uniform thermal gradient.

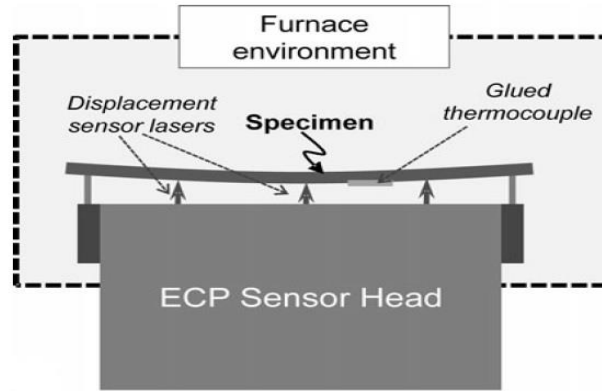


Figure 1-13. Schematic of curvature - temperature measurement device, ex-situ coating property (ECP) [64].

After recoding the curvature and temperature changes during thermal cycling, the curvature - temperature data is determined, via an inverse analysis technique, required parameters are calculated to evaluate the complete stress-strain relation of the coating (See Fig. 1.14). Based on the stress–strain relationship, three key parameters which quantify the anelastic behavior of coating can be defined. The first parameter is “elastic modulus of coating E ”, the slope between the minimum point (at room temperature) and the transition point corresponds to the change from linear to nonlinear relations. The second is “Nonlinear Degree (ND)” to quantify the extent of nonlinearity of stress-strain curve (ND) is determined from the ratio of E at low strain over a secant elastic modulus E_s at elevated temperature ($ND=E/E_s$). E_s represents the tangent modulus at a higher temperature (the slope between the transitional point and the point at additional 0.1% strain). In fact, E describes the coating's stiffness at low strain which is related to the coating's integrity and strength of the interlayer bonding, while ND characterizes the flexibility of coating at elevated temperature. The third anelastic property is introduced as “Hysteresis Degree (HD).” This parameter is obtained from the ratio of enclosed area (A) of stress–strain curve over the rectangular area given by $\Delta\epsilon \times \Delta\sigma$ ($HD= A/\Delta\epsilon \times \Delta\sigma$) which determines the relative energy

dissipation during thermal cycling due to frictional sliding of coating's interfaces[50, 63,64]. These three parameters, E, ND, and HD, are unique for every coating which has its own defect architecture. In fact, the anelastic parameters and coating microstructure can be considered as a coating signature for desired application. Although it is not possible to achieve exactly identical microstructures in two different coatings with the same spraying parameters, the specific anelastic behavior of each coating permits to evaluate their mechanical response under different loadings.

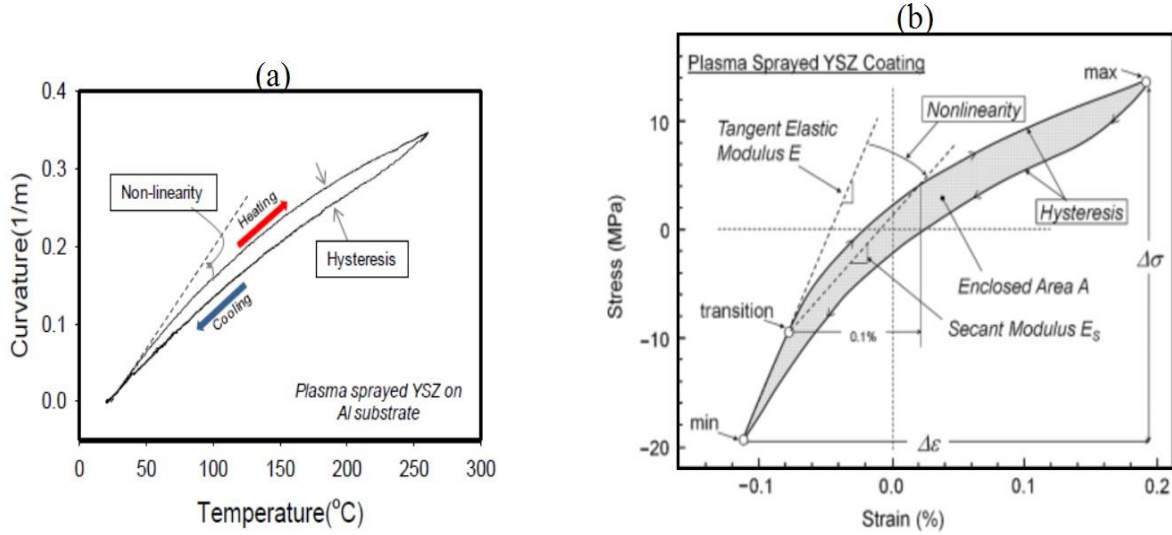


Figure 1-14. Anelastic behavior of plasma sprayed YSZ on Al substrate. a) Nonlinearity and hysteresis of curvature-temperature plot when subjected to thermal loading [66]. b) Nonlinearity and hysteresis in stress-strain relationship, and also key parameters of anelastic behavior[50].

The curvature measurement under temperature change offers several advantages compare to other measurement techniques of coating's modulus. Unlike other standard mechanical loading methods such as tensile and three-point bend tests in which stress concentration is limited to a specific area, thermal loading in ECP measurement offers more uniform stress along the samples and deformation states which are more ideal for property measurements. Since there is no post-deposition sample preparation in ECP method, it provides more precise and non-destructive measurement of coating properties. And also, less effective measurement error on coating's properties compares to other mechanical loading tests can be considered as the main advantages of substrate curvature measurement method. In short, as it is possible to estimate the stiffness and durability of coating at low strain, and also evaluate the flexibility of ceramic coatings at high operating temperature. The applied method can be suitable for determining the desired quality for a given coating used as TBC.

1.6. Objectives

As discussed, suspension plasma spray (SPS) technology is a novel method to produce ceramic coatings with submicron size particles providing enhanced properties for thermal barrier coating application. Since many processing parameters are involved in the manufacturing of SPS coating, the first goal of the current study is to produce different YSZ coatings with submicron-scale particles through changing the spraying parameters by various means, such as spray distance, plasma enthalpy and spray velocity to evaluate the effect of each parameter on the coating microstructure. Coatings with columnar features and segmentation crack structure for TBCs application is considered as our target. Based on previous experiences and results, some spraying parameters have been chosen to reach to the desired coating structure.

As mentioned, the previous researchers investigated the anelastic properties of ceramic coatings manufactured with regular plasma spray. Since there is evident lack of studies focusing on the anelastic behavior of suspension plasma sprayed YSZ, the second objective of this thesis is to investigate the anelasticity of SPS coatings exhibiting significant differences in the coating microstructure through substrate curvature measurement device, ex-situ coating property (ECP) sensor.

2. Experimental procedures

In this chapter, the experimental procedures of suspension plasma spray, and ex-situ coating property (ECP) sensor will be discussed in detail, separately.

So, in the first section, the SPS process includes substrate and suspension preparation, suspension feeding mechanism and torch raster pattern applied in this study, and also the metallographic preparation of sprayed coatings will be explained step by step.

In the second part, the mechanism of ECP sensor comprising components function, thermal cycling (heating and cooling procedure), data acquisition and quantification of anelastic properties by using non-linear model and the curvature-temperature plot will be described.

In the last part of this chapter, the function of anelasticity parameters for the plasma sprayed ceramic coatings as an index for correlation between mechanical properties and microstructural features will be mention.

2.1. Substrate Preparation

All coatings were deposited on the 304 stainless-steels with a squared shape of 25.4 x 25.4 mm² and thickness 3.5 mm to evaluate the microstructure of the suspension plasma sprayed coatings. First, the substrate surfaces were cleaned with alcohol to eliminate contamination, particularly from oil or grease (See Fig. 2.1 from (a) to (d)). The Substrates in a uniform and controlled condition were grit blasted into a cabinet using aluminium oxide (Al_2O_3) with the particle size of $\sim 200\text{ }\mu\text{m}$ at 40psi. Grit blasting process increases the substrate surface roughness through providing asperities or irregularities on the substrates surfaces improving adhesion between the coating and substrate [3]. The substrate surface roughness $R_a \sim 4.25\text{ }\mu\text{m}$ was computed with a 3D confocal laser microscope (Olympus OLS4000). In the final step, the substrates are cleaned by blowing compressed air jets to remove embedded grit residues on the surface as much as possible to decrease the coating-substrate interface defect and improve adhesion.

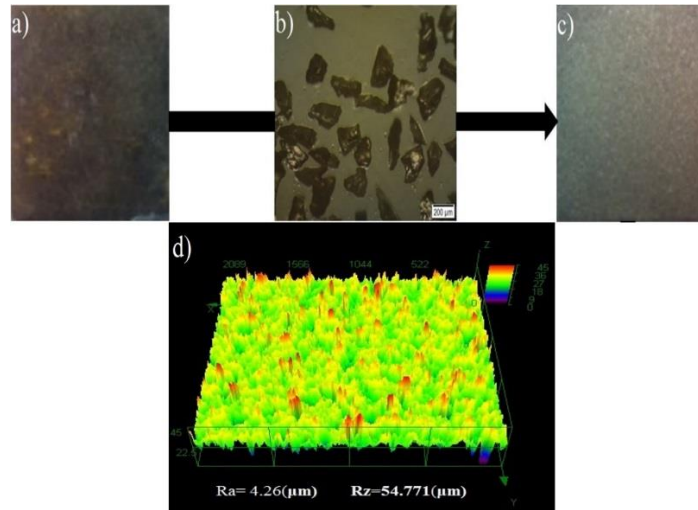


Figure 2-1. Substrate preparation steps. a) stainless-steel before cleaning and grit blasting. b) Aluminium oxide (Al_2O_3) for grit blasting with particle size of $\sim 200\text{ }\mu\text{m}$. c) Substrate (stainless-steel) after cleaning and grit blasting. d) Substrate roughness measurement with 3D laser microscope.

2.2. Suspension preparation and characterization

As discussed in the previous chapter, compliance of yttria stabilized zirconia (YSZ) for thermal barrier applications has been accepted by the industry. The ceramic material utilized during this study contained zirconium oxide (ZrO_2) powder (Changsha Huazun Ceramic Material Co, China) stabilized with 5 mol% (8 wt %) yttrium oxide, also known as yttria (Y_2O_3). To prepare the

suspension, ethanol was selected as the solvent based upon low toxicity, availability, and less enthalpy to vaporize it compared with water [15,19,29,34]. Submicron particles, especially oxides have a tendency to agglomerate due to electrostatic attraction resulting in increasing the sedimentation rate [65, 66]. The particle agglomeration and sedimentation is hindered or delayed by using 5wt% of YSZ polyvinylpyrrolidone (PVP) as a dispersant which adsorbs on the particle surface and provides effective particle dispersion by presenting long polymeric chains. Once the ethanol-dispersant solution is well mixed by using a magnetic stir bar, the YSZ powder is gradually added to a concentration of 20 wt% of YSZ in suspension(See Fig. 2.2). To provide better dispersion and prevent agglomeration an ultrasonic agitator was used during suspension preparation.

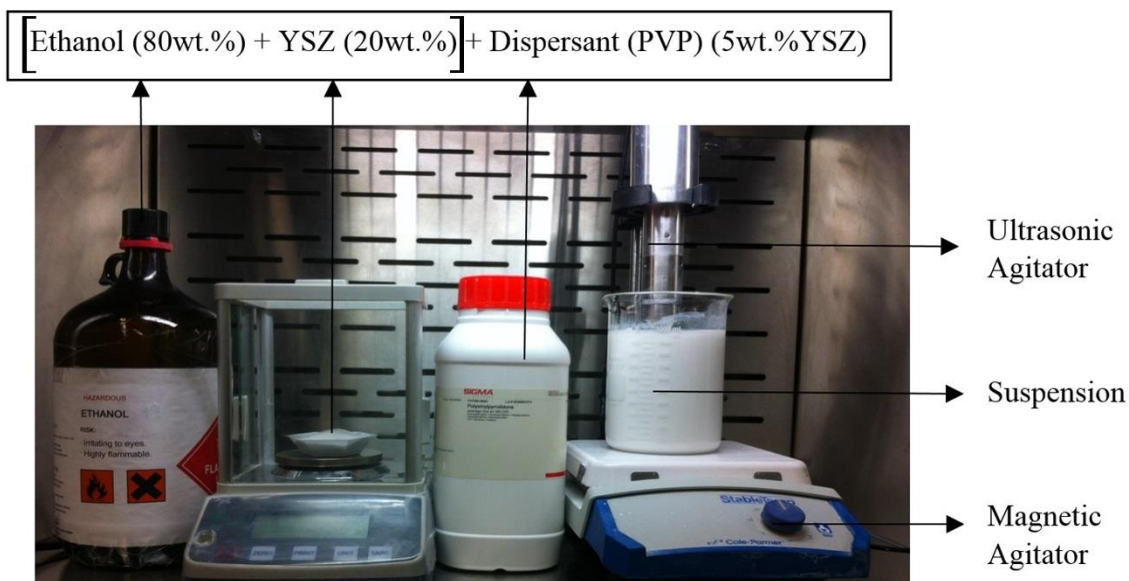


Figure 2-2. Suspension preparation contents and formulation.

Suspension characteristics regarding viscosity, surface tension, and particle size distribution have a significant influence on the atomization process and thermal treatment of particles within the plasma jet [17, 25, 65–67]. The investigation of the effect of each mentioned suspension factor on the coatings quality is beyond the scope of this study, and it should be mentioned that all suspension properties have been held constant within these experiments.

Size distribution of the dispersed particles in the suspension was measured by a laser light scattering technique (Spraytec, Malvern, UK), and the average particle size was

$D_v(50) = 0.385 \text{ (}\mu\text{m)}$ (See Fig. 2.3.a). Also, suspension viscosity measurement was performed through glass capillary viscometer (Cannon-Fenske Opaque Viscometer, Fisher Scientific, USA), and the measured dynamic viscosity was 5.2 (mPa-s). To rely on the capillary viscometer results, the viscosity measurement was also accomplished by automatic rheometer instrument (MCR Rheometer, Anton Paar, and CANADA) (See Fig. 2.3.b). The suspension must have relatively low viscosity and good stability (without agglomeration) to avoid clogging issues and provide an easier liquid injection into the plasma plume. The suspension viscosity decreased to 4.2 (mPa-s) by drying the YSZ powder inside a muffle furnace for 1hr at 120 °C to reduce the humidity level of powder and also the risk of agglomeration. The next measured suspension character was surface tension, which was performed with a tensiometer (Interfacial Tensiometer, Fisher Scientific, USA). Table 2.1 shows the summary of all suspension properties utilized for producing SPS coatings in this study.

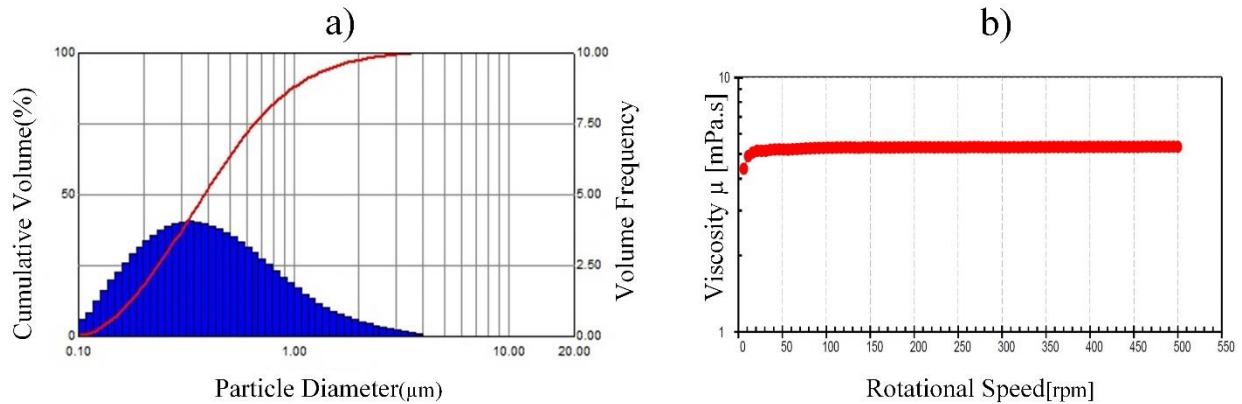


Figure 2-3. Suspension characteristics. a) Particle size distribution through laser light scattering technique, showed average particle diameter $D_v(50)=0.385(\mu\text{m})$. b) Suspension viscosity measurement result by automatic rheometer instrument provided a dynamic viscosity of 5.25 (mpa-s)

Table 2-1. Summary of suspension properties measurement

Suspension Properties	Viscosity(mpa-s)		Density (g/mL)	Surface tension (N/m)	Particle D_{50} (μm)
	Without drying	With drying			
20wt.%YSZ	5.2	4.2	0.85	0.025	0.385

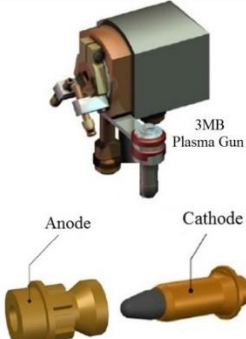
2.3. Procedure of suspension plasma spray process

2.3.1. Plasma generation

The torch used for plasma generation consists of two water-cooled electrodes namely the anode and the cathode, a finger-shaped tungsten cathode partially contained into a cylindrical copper anode generating an electrical arc due to the voltage breakdown between both electrodes. The most frequently plasma-forming gases which are introduced from the back of the torch interior are argon (Ar) as a primary gas to stabilize the arc inside the nozzle, and hydrogen (H₂) or helium (He) as secondary gas, to increase the power density, gas velocity, and the heat transfer rates to powders. The electric arc heated the gas molecules to form a plasma plume and the generated plasma comes out of the torch at high speed due to gas expansion. Based on the required coating conditions, the composition of the gasses is selected.

The coatings presented in this study were sprayed by using 3MB plasma torch (Oerlikon-Metco, Switzerland) with a 20 mm long anode with two different internal nozzle diameters (5 mm and, 8 mm), and it was mounted on a six-axis robot. Two different gas mixtures, Ar/He (25/25slpm) and Ar/H₂ (45/5 slpm) were used for plasma generation. However, the most predominant plasma gas was argon/helium mixture since in comparison to H₂, He increases the thermal conductivity and decreases the fluctuations of the plasma plume and also its high viscosity up to about 14000 K results in a reduction of the mixing with the surrounding air, generating larger and more stable plasma jets[68]. The main torch characteristics are summarized in Table 2.2.

Table 2-2. Main characteristic of 3MB plasma gun

	Properties and features
	<ul style="list-style-type: none">• Power Capability: optimum performance at levels of 40 kW (100 % duty cycle)• High heat output capabilities: plasma gas temperatures up to 16000 °C (28880 °F)• High plasma gas velocity: in excess of 3050 m/s(10000 ft/s)• High particle velocities: up to 610 m/s (2000 ft/s)• Max. Plasma Current [A] <750 - Max. Plasma Voltage [V] <75

2.3.2. Suspension feeding mechanism

The suspension injection method is considered as a main parameter in the SPS process and has to be adjusted with the required accuracy to produce a homogeneous treatment of solid particles in the plasma plume. In fact, the suspension can be injected mechanically into the plasma plume from outside of the nozzle (external injection)[16] or from inside the nozzle (internal injection)[23] depending on the plasma torch design. In this study, only the case of an external injection will be considered and discussed. The suspension feeding mechanism includes two sealed tanks in which the suspension and solvent are stored separately. A stainless steel suspension injector with the internal diameter of 150 μm was oriented with the 15° angle with respect to the vertical axis. The injector axis is positioned in such a way that the flow of suspension jet penetrates the plasma at counter-flow, and targets the nozzle axis at the exit of the nozzle (See Fig. 2.4). Moreover, the injector tip is accurately adjusted close to plasma torch orifice at a distance of 25 mm from the torch axis by a micro-positioning system installed next to the injector holder.

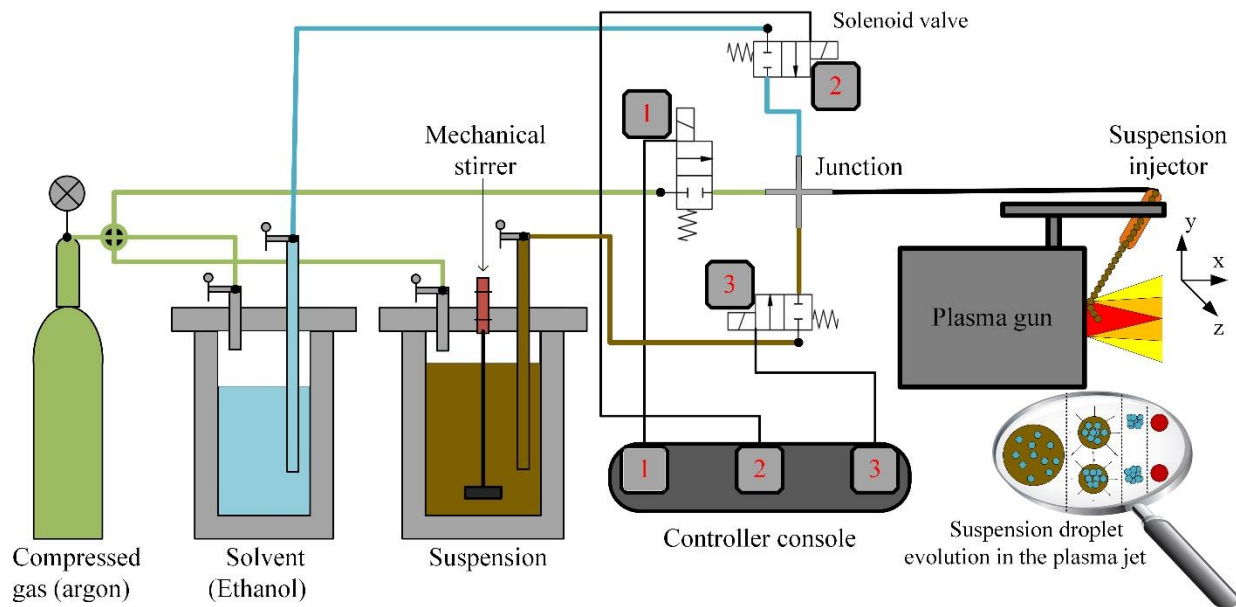


Figure 2-4. Schematic description of suspension feeding system.

A mechanical stirrer is used to avoid the sedimentation of the solid content in the suspension during deposition. A compressed gas (argon) at 60 psi, pressurized the suspension and solvent containers by changing their levers to the open position. A set of solenoid valves, which are attached to an extension holder and fixed to the rear of the robotic arm is adjusted through using a controller

console installed outside the spraying cabin. By switching on the solenoid valve number 3, the suspension is introduced to the injector and plasma plume with a 20 ml/min mass flow rate. The continuous liquid jet penetrates the plasma plume and after fragmentation/vaporization, the YSZ particles treated in the plasma plume and are propelled toward the substrate, and form the coating. After shutting down the process, in order to ensure the repeatability of experiments and avoid injector clogging issues, by interval switching on solenoid valve number 1 and 2, compressed gas (argon) and solvent pass through the suspension pipes, respectively to clean the suspension residue.

2.3.3. Coating deposition and torch raster pattern

Through scanning the plasma torch over the substrate in a plane parallel to the surface, deposited particles (splats) form a bead. The overlapping and stacking of deposited beads in each pass make a coating's layer (See Fig. 2.5 a). In fact, the plasma plume into which the suspension is injected can be divided into three main regions: (I) hot inner core, (II) moderate temperature area close to the jet core, and finally (III) cold temperature on the plasma periphery [69]. Thereby, the surface of the deposited bead can be divided into well treated particles (i.e., fully molten) forming dense region upon impact and spreading (bead central part) and also, poorly treated particles traveling in the jet fringes and low temperature regions of the plasma flow embedding in the coating structure (bead edges) as a defect[70]. The degree of particles melting in the plasma flow and their travel trajectory toward the substrate depends on SPS process parameters. This means that the density of well-treated particles in the center of bead and also semi-molten/unmolten (overspray) particles in its wings vary corresponding to the process parameters such as plasma enthalpy, suspension feeding rate, torch speed and stand-off distance which will change the droplets fragmentation/vaporization rate significantly. Thereby, different coating microstructures regarding defect size, shape, and their distribution within the coating can be manufactured by changing the process parameters.

Coating's layers, as with conventional spraying, are made by overlapping beads. Once the first bead is deposited during one stroke, the torch is translated in the vertical direction corresponds to specified overlapping ratio to spray the next one on the substrate surface and previously deposited bead. So, one pass is defined as multiple strokes to coat a complete layer. With such determined bead overlapping the central dense region of deposited bead covers the preceding bead edges partly

which is less dense than the bead central part, and also, the dense part of the former bead expose to the part of the deposited bead, which is made by the material coming from colder regions of the plasma, and so on[69–71]. Each complete pass of the coating results from successive beads overlapping with a mixture of the deposited particles from both the hot and cold regions. The powdery material, re-solidified particles, and overspray deposit (see Sect. 1.3 for details) embedded in the coating structure have an effect on the quality of inter-splat/inter-layer bonding strength.

In this study, to deposit YSZ powder through suspension injection into the plasma plume, the plasma torch was moved by a robot arm in a raster pattern with a meander-like movement (See Fig. 2.5 b). During deposition, the substrates were kept stationary, while the plasma torch was translated in the x-direction with a constant speed (1 m/s or 0.5 m/s) and a specified stand-off distance (30 mm or 50 mm) with respect to the substrate surface. Once a bead was deposited, the plasma torch was indexed in the y-direction (3 mm) for the next adjacent bead. To cover the entire substrate surface, the torch scanned the surface with an additional tolerance of 10 mm in each horizontal displacement. Depending on different spraying parameters which will be discussed in the following section, the deposition rate varied from 2 μm to 6 μm per pass. Coatings were sprayed between 20 and a few hundred passes resulting in thicknesses between 50 μm to 0.5 mm.

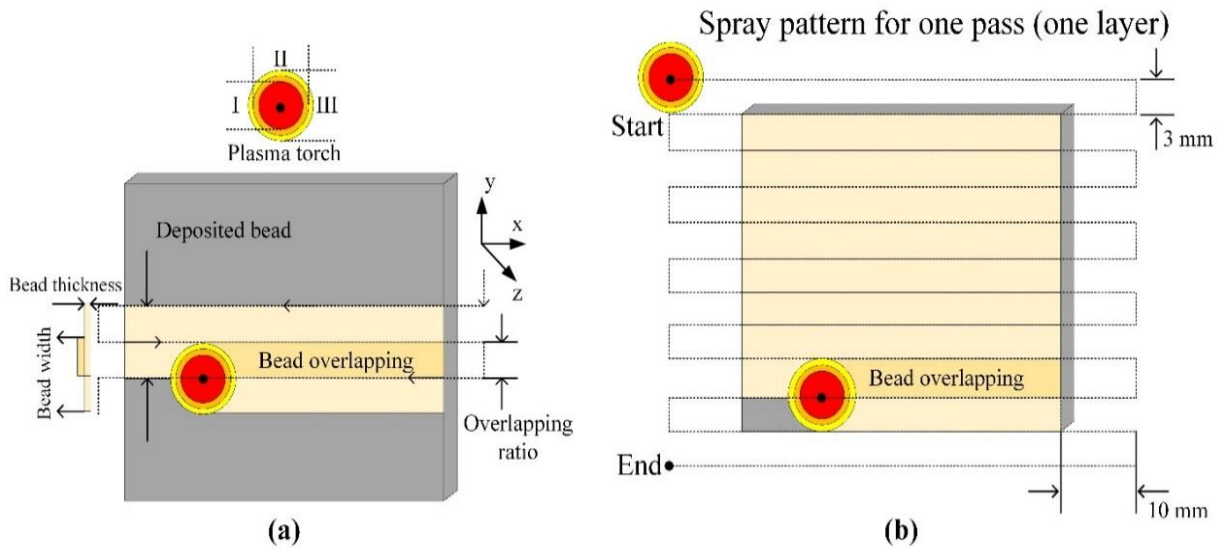


Figure 2-5. Schematic description of torch raster pattern. a) Representation of the plasma torch with different temperature regions scanned over a flat surface and bead overlapping formation mechanism. b) Spray pattern for one coating pass used in this study.

2.3.4. Design of experiments for suspension plasma spray process

To manufacture YSZ ceramic coatings through SPS process, six different spraying conditions were defined to obtain dissimilar coating structures. To evaluate the effect of spraying parameters on coatings microstructure and deposition rate, one set of parameters (stand-off distance: 30 mm, torch raster velocity: 1m/s, plasma gas mixture: Ar/He (25/25slpm), I: 600 Amp, V: 40 Vol, and nozzle diameter: 5mm) was considered as a reference (T1), and through changing a specific factor in each test, five other (T2(LS)-T6(ID)) runs were designed (See table 2.3). It should be noted, in all experiments, suspension properties (viscosity, surface tension, and density), and also injection condition (suspension mass flow rate, angle, and velocity) were constant, and just through altering the plasma torch condition in terms of gun raster speed (LS), torch-substrate distance (HD), plasma gas composition (GC), power (enthalpy) (HP), and internal nozzle diameter (ID), five different runs were planned. It is clear that the efficiency of heat transfer and momentum from the plasma to the droplets and substrate will be influenced by using different plasma torch conditions. The effect of each specific parameter on the coatings microstructure and deposition rate will be discussed separately in details in chapter 3.

Table 2-3.Process parameters of suspension plasma spray

TEST NO	Stand-off Distance mm	Spray Velocity M/S	Plasma Gas			Current Amp	Voltage Vol	Power KW	Nozzle Diameter mm
			Ar	He	H ₂				
			LPM						
T1 (Ref)	30	1	25	25	-	600	40	24	5
T2 (LS)	30	0.5	25	25	-	600	40	24	5
T3 (HD)	50	1	25	25	-	600	40	24	5
T4 (GC)	30	1	45	-	5	600	56	33.6	5
T5 (HP)	30	1	25	25	-	700	40	28	5
T6 (ID)	30	1	25	25	-	600	40	24	8

2.4. Coatings characterization

2.4.1. Metallographic preparation of sprayed coatings

In order to study and evaluate the microstructure of all sprayed coatings through scanning electron microscope (SEM), consecutive processes including cold-mounting, sectioning, and grinding-polishing, were applied, respectively in the following details:

Cold-mounting: Before sectioning, to manipulate samples easily and protect their edge during cutting, sprayed samples mounted through using rubber cups as a mold and epoxy (ANAMET, CANADA) comprising a resin and a hardener (volume ratio 7 parts resin to 1 part hardener) as a curing material. To elaborate the epoxy infiltration along coating interconnected pathways, and evacuation the possible bubbles within the epoxy, a vacuum system (Cito Vac, Struers, Canada) used which is including a round vacuum chamber to place the molds in a circular pattern, and also a container to pour the mixed epoxy around the specimen through a disposable inlet tube in the cups (10 min at a pressure of 10 Kpa). After curing (5 hours), molded samples can be removed easily from the cups which have detachable bottoms.

Sectioning: To provide a cross-section of sprayed samples for grinding/polishing process, a cut-off machine (Secotom-15, Struers, Canada) was used. Mounted sample fixed within the holder placed on the movable table. In fact, it should be positioned in such a way that sectioning of the coating begins from the center line of sample parallel to spray direction, and from the outermost layer of the coating, inward and through the substrate. In this approach, the cutting-wheel will produce a compressive stress in the sample rather than a tensile stress, thereby preventing the coating from delamination. A compatible cutting-wheel selected according to the hardness of ceramic material (50A20, $200 \times 0.8 \times 22$ mm, Struers, Canada). To start the cutting process, the machine was programmed with 2000 rpm for cutting-wheel, and 0.5 mm/s feed rate for movable table, and also by measuring the mounted sample diameter, the total feeding length was defined 35 mm for all samples. To protect the machine from corrosion, and to improve cutting and cooling properties, a flow of mixing of water and lubricant (Corrozip, Struers, Canada) in defined ratio was used during operation.

Grinding and Polishing: in order to reach a surface suitable for observation at both low and high magnification, the prepared metallurgical samples were then placed into a series of automatic grinding-polishing machine (Tegramin-25, Struers, Canada). Six sample mounted symmetrically

into the specimen holder which is attached to the head of machine. Both head and platen of the machine are capable of rotating in clockwise or vice versa. A continuous water flow was used during the process as a coolant, which also flush away the surface removal products. The grinding process was firstly performed from the coarse abrasive silicon carbide papers (240 and 400 grit) in order to remove the deformation and cutting-wheel marks produced during sectioning. Then, the fine silicon carbide grinding papers (600 and 1200 grit) were employed to attain an acceptable flat surface for polishing. The final stage was polishing in which the abrasive paper replaced with the polishing cloth, and also a series of diamond abrasive suspended in water-soluble oil (9,3 and 1 μm) used to remove any deformation resulting from grinding, and to reach a mirror-like surface. The summary of grinding-polishing steps is listed in the following table.

Table 2-4. Grinding and polishing steps with specific parameters

Step Set up	Silicon Carbide (Grit 240)	Silicon Carbide (Grit 400)	Silicon Carbide (Grit 600)	Silicon Carbide (Grit 1200)	Water-based diamond suspension particle size (9 μm)	Water-based diamond suspension particle size (6 μm)	Water-based diamond suspension particle size (1 μm)
Time (min)	2	2	2	2	3	5	5
Platen speed (rpm)	300	300	300	300	300	300	300
Head speed (rpm) Opposite to platen	150	150	150	150	150	150	150

2.4.2. Scanning electron microscope (SEM) analysis

The cross-section of polished samples were investigated through a variable pressure scanning electron microscope (SEM, Hitachi, S-3400N). The coating cross-section was coated with a carbon film to achieve electrical conduction of observed surface. The mapping of micro-regions was conducted through a backscattered electrons (BSE) 3D detector at voltage 15 KV, pressure 50 Pa, probe current 40 Amp, and at a focusing distance of 5 to 10 mm, allowing for magnification of up to 2500X used in this study.

2.5. Experimental procedure of ex situ coating property (ECP) sensor

2.5.1. Specimen preparation

After evaluation the SEM images of YSZ coatings microstructure produced in six different spraying parameters, three sets of them with different coating characteristics were selected for further mechanical properties measurements. To perform thermal cycling test with the ECP device, six grit blasted, and heat treated 304 stainless-steel samples with the rectangular shape of 230 mm x 25.4 mm x 1.55 mm were sprayed with the customized sample holder provided by Stony Brook University (See Fig. 2.6). To assess the repeatability of coatings anelastic parameters, two samples were sprayed for each constant processing conditions. The substrate temperature during deposition was recorded by using a K type thermocouple (HHM9007R, OMEGA Inc., USA). To avoid any erroneous values for temperature due to air flow through the gap between the thermocouple and the substrate, the thermocouple wire was fixed and cemented (CC High-Temperature Cement, OMEGA Inc., USA) on the center of the uncoated side of the samples.

It should be noted that, as suspension injector was clogged in many times during deposition on small samples due to high dynamic viscosity 5.2 (mPa-s), its viscosity decreased through drying the powder before preparation of suspension for this set of experiment.

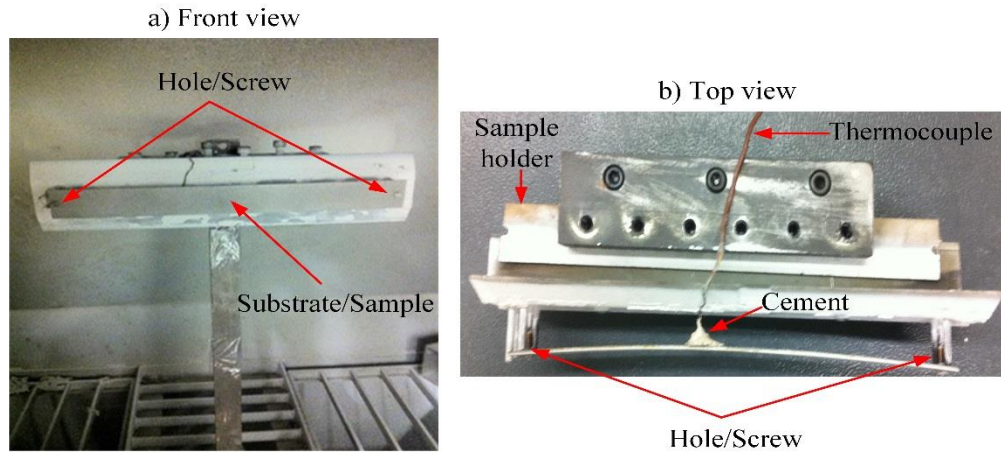


Figure 2-6 Substrate and sample holder with the thermocouple. a) Front view. b) Top view

2.5.2. Coating thickness measurement

Coating thickness is considered as an input parameter for quantification of anelastic parameters. So, after ECP test, all samples were cut from two area to evaluate the coating thickness distribution

along the sample, and to measure the mean value of thickness for analysis. The coating thicknesses were measured through a microscope to achieve more precise results (See Fig. 2.7). Two sections, close to the center and the edge (near to the hole in which the screws fastened) were cut from each sample. Under microscope each section divided into three zones again left (top), center and right (bottom), then in each zone 10 distance were measured randomly (totally 20 measurements for each zone).

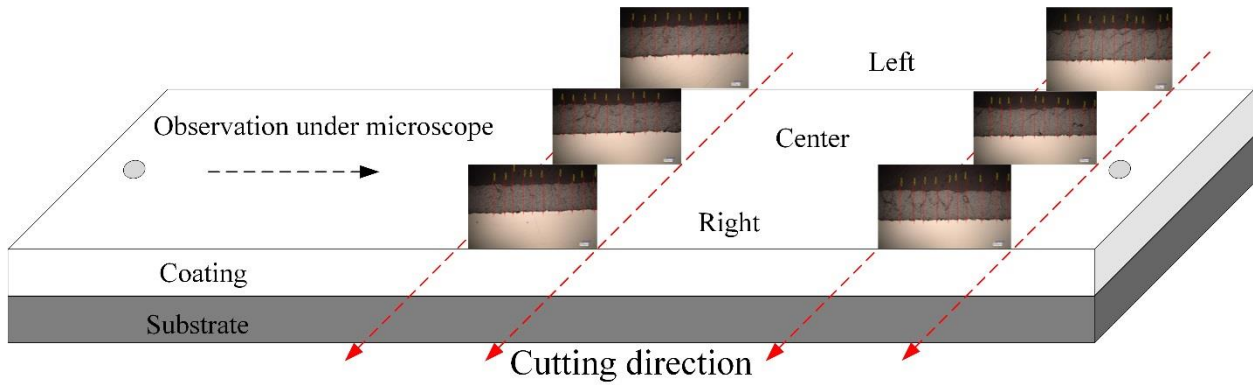


Figure 2-7. Coating thickness measurement under optical microscope

2.5.3. Bilayer curvature-temperature (BCT) measurements

2.5.3.1. Experimental setup

The ECP setup, including a box with channels which provides a uniform heating and cooling with a negligible thermal gradient of 1 to 2 °C both in through thickness as well as along the length directions. As the lasers can function up to a maximum temperature of 40°C, a water chiller has also been installed to facilitate the thermally cycling through circulating water within the channels inside the box. To measure temperature variation during heating and cooling cycles a K-type thermocouple is welded on the back side of the substrate. To start the experiment, the specimen is mounted vertically on ECP sensor with the screws fastened through two holes on both sides of the substrate such that the laser beam projected on the coated side (See Fig. 2.8). The laser reference point is set on the zero, and the furnace temperature is adjusted to the required maximum temperature which was 570°C for the case of YSZ coating on stainless-steel. Then, the coated substrate is heated inside a muffle furnace (Thermolyne- F6018) up to the adjusted maximum

temperature for almost 40 min ($\sim 0.3^{\circ}\text{C/s}$). At the end of the heating cycle, the furnace is turn off automatically, and it is cooled down back to the room temperature which is taking approximately 8 h. Due to CTE mismatch between the coating (YSZ) and substrate (stainless-steel), the curvature of specimen changes with temperature. The stainless-steel with a CTE of $16\text{ }\mu\text{m/m-}^{\circ}\text{C}$ tends to expand more than the ceramic YSZ with a CTE of around $10\text{ }\mu\text{m/m-}^{\circ}\text{C}$. To accommodate this thermal strain misfit the beam bends. The curvature is calculated from a radius of the circle that fits the beam deflections measured by three separate laser displacement sensors (SUNX LM10, Japan, resolution $\sim 1\text{ }\mu\text{m}$) with their measurement axes perpendicular to the specimen. The curvature-temperature collected data is recorded and processed through data acquisition box and transferred to the computer for further analysis by using CTSR's in-house software Kurvaware.

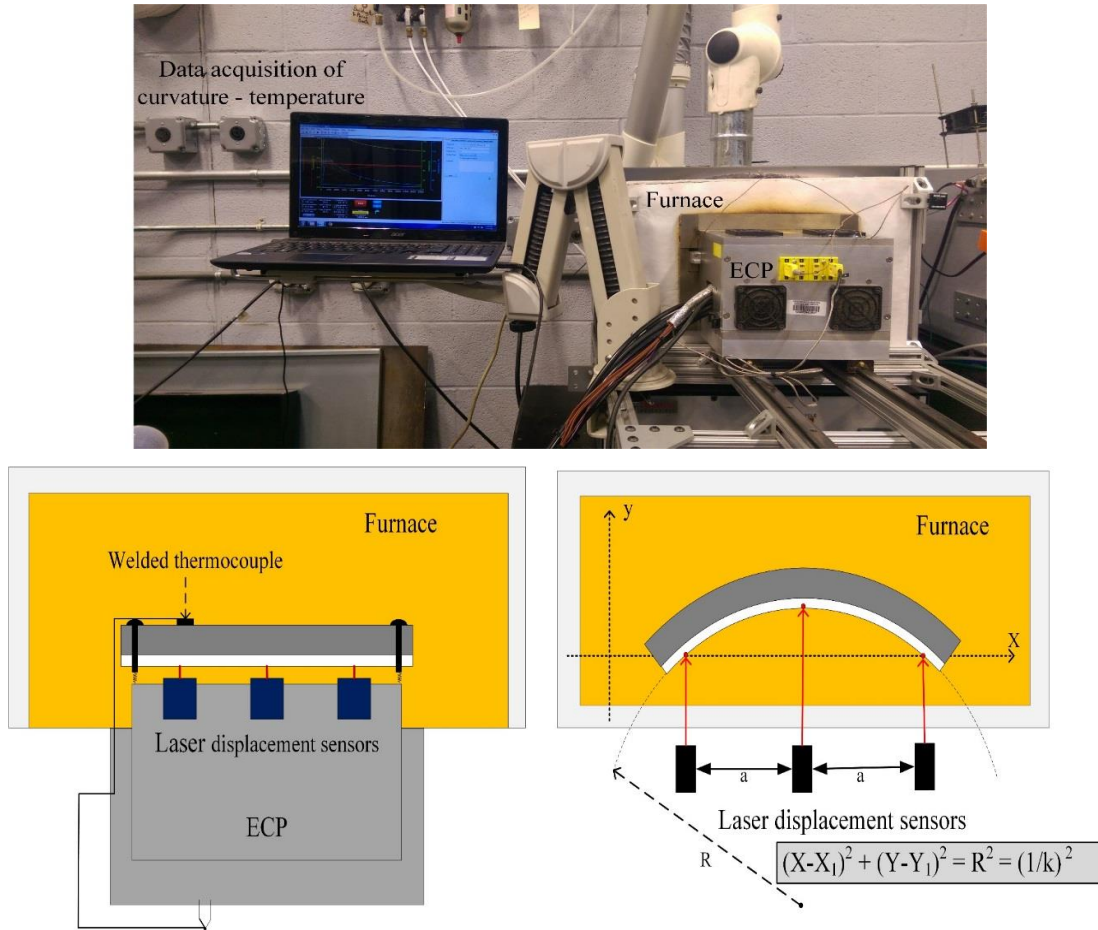


Figure 2-8. The photograph and schematics of ECP device which is thermal cycling the beam through using a muffle furnace. Measure the temperature and curvature of the specimen using welded thermocouple and three laser displacement sensors, respectively.

For each specimen, multiple thermal cycles were performed to achieve repeatable curvature-temperature responses for nonlinear properties analysis of coating. To plot the curvature-temperature curve for each cycle, a program was written and prepared in visual C++ to reduce the number of data points of curvature and temperature. The program was just based on avoiding the data within a change of 1°C (after rounding off the temperature data) (See Fig. 2.9). It should be noted, in all cases the first cycle was not similar to the consecutive ones, and also in some thermal cycles there was an uneven path during heating which was likely related to the accumulation of foreign media such as moisture, dust or even water droplet on the laser window which can result in decreasing the intensity of laser and data accuracy. To analyze the curvature-temperature responses and calculate the anelastic parameters, those cycles which were exempt from any noise and disturbance were considered as applicable cycles for analysis.

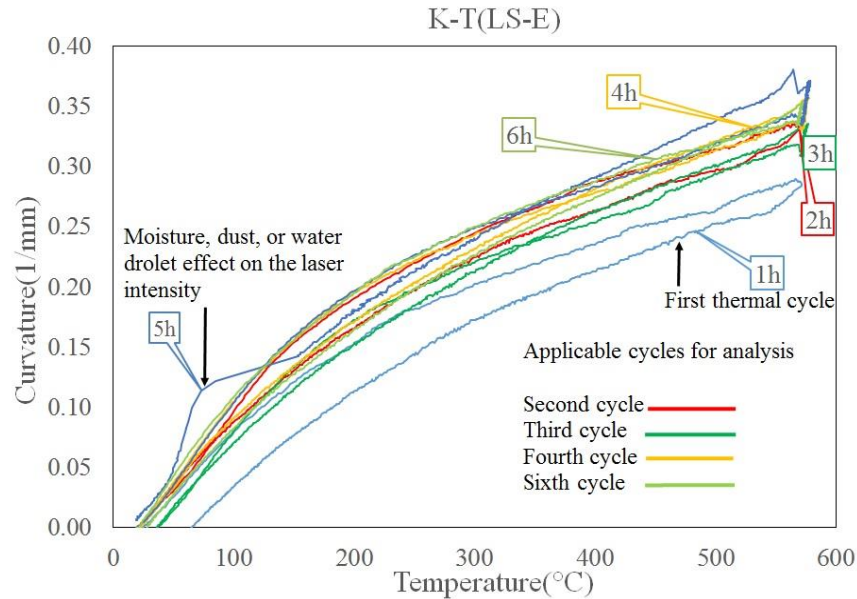


Figure 2-9. A repeatable curvature-temperature plots obtained from heating and cooling both in the furnace for one sample. First cycle (1h) is different from the consecutive cycles. Also in this specimen during fifth cycle (5h) in the heating part, foreign media decrease the lasers intensity, and interfere the data points in a region.

2.5.3.2. Quantification of anelastic properties by using non-linear model and curvature-temperature plot

Elastic modulus at low temperature, the nonlinear degree of curvature-temperature curve, and its hysteresis degree are three anelastic coatings properties which can be quantified through plotted curves. For each specimen, those curvature-temperature responses, which were applicable for

further nonlinear properties quantification, were selected. For example in case Fig2.7 the second (2h), third (3h), fourth cycle (4h) and sixth cycle (6h) designated as a reference to analyze the anelastic parameters of the coating. It should be noted, in a heating-cooling cycle, the cooling rate is highly dependent on environmental conditions as the beam cool down to the room temperature inside the furnace, and it can vary from day to day for the same furnace setting; therefore only heating curve which is under controlled condition will be used to assess the non-linear properties of coatings. From the heating cycles, the temperature range across which the analysis is to be executed, and the transition temperature beyond which the nonlinearity in the coating started, can be extracted (See Fig. 2.10). The transition point is selected manually through drawing a straight line along the curvature-temperature plot from the minimum temperature with the maximum number of data point contacting on the line.

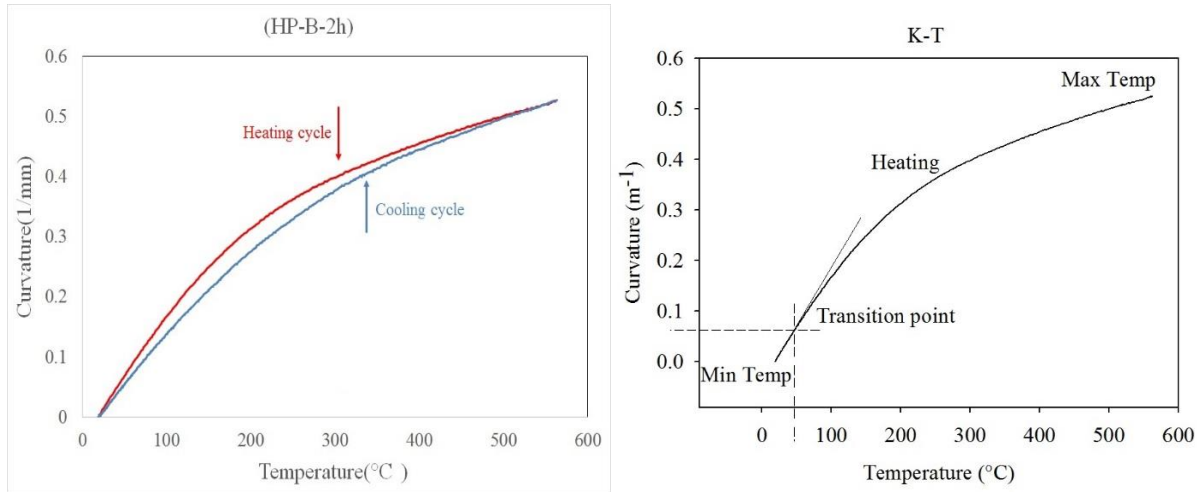


Figure 2-10. Initial steps to quantify the anelastic properties of YSZ coatings. The selected repeatable curvature-temperature response which is qualified for further analysis. The heating curve of thermal cycle is plotted separately to determine the temperature range over which the thermal cycle was performed, and to select the transition point in which the curve started its nonlinear behavior.

Apart from the acquired temperature data from heating cycles, there are some other input parameters including coating and substrate thickness, elastic modulus of substrate (200 Gpa for stainless-steel) and coefficient of thermal expansion (CTE) of both coating and substrate are required as input parameters for the analysis. To quantify the nonlinear properties of suspension plasma sprayed YSZ coatings, all these collected data transferred to a phenomenological constitutive uniaxial stress-strain model proposed by Nakamura et al [59,72]. The proposed procedure is based on modified Ramberg–Osgood nonlinear stress– strain relation, and utilizes nonlinear bi-material beam solutions as well as an inverse analysis in which the Kalman filter is

used. In this model, the elastic modulus of the coating at linear segment of curvature-temperature curve, is calculated from Eq.(2.1): [73].

$$\Delta K = \left[\frac{6 E_C E_S t_C t_S (t_C + t_S)}{E_C t_C^4 + E_S t_S^4 + E_C E_S (6 t_C^2 t_S^2 + 4 t_C^3 t_S + 4 t_C t_S^3)} \Delta \alpha \right] \Delta T \quad \text{Eq. (2.1)}$$

Here, t_C and t_S are the thickness of coating and substrate, respectively, and E_S and E_C are the elastic modulus of the substrate and coating, respectively. $\Delta \alpha$ is the difference in thermal expansion coefficients of substrate α_S and coating α_C , and ΔT is the temperature change in the linear section. The above equation with measured ΔK _ ΔT record is used to determine the coating modulus E_C at low strain in linear segment. The ratio of the measured elastic modulus at low temperature E_C , and E_{sec} which is defined as the secant modulus, and the slope between the transition point and the point at additional 0.1% strain in nonlinear segment of stress-strain curve to approximate the relative degree of nonlinearity of curvature-temperature curve (See Fig. 1.14.b for details)[50, 60].

$$ND = \left(\frac{E_C}{E_{sec}} \right) \quad \text{Eq. (2.2)}$$

From the curvature-temperature plot, another parameter “Hysteresis Degree (HD)” can be extracted to complete the quantification of anelasticity in a coating[50,63]. This parameter is calculated from the ratio of enclosed area (A) of curvature-temperature curve over the rectangular area given by $\Delta K \times \Delta T$ (i.e., $HD_{K-T} = \left(\frac{A_{K-T}}{\Delta K \times \Delta T} \right)$) (See Fig. 2.11).

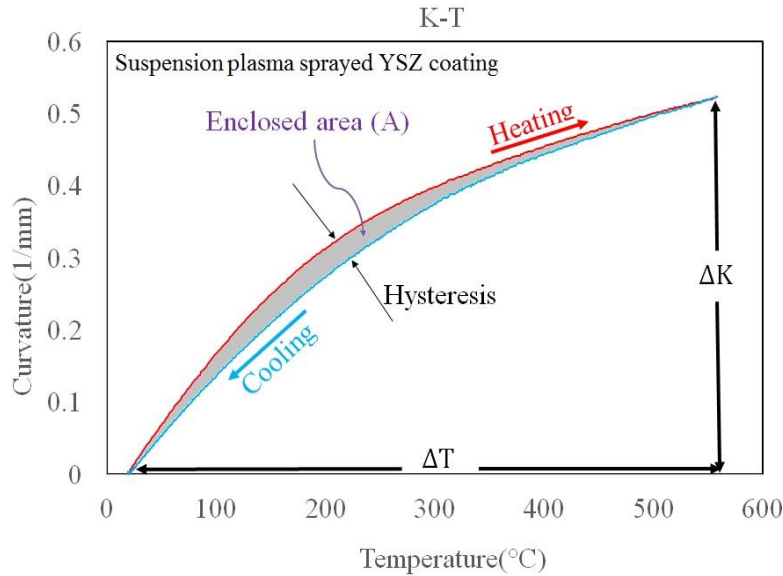


Figure 2-11. A typical curvature-temperature plot obtained from ECP measurements for a SPS YSZ coating. Hysteresis behavior between heating and cooling cycle, and related parameters to calculate hysteresis degree.

2.5.4. Anelasticity parameters function

Three anelasticity parameters E, ND, and HD can provide insights into the coatings properties and microstructure. In fact, it should be possible to establish a correlation with coating's processing conditions, and its microstructural features through a comprehensive understanding of these anelasticity parameters.

The elastic modulus of the coating (E) represents the coating initial stiffness at lower strains when most of the microstructural defects are compressed or immobile[50]. In other words, the stiffness of a coating means how much it can deflect under a given load (thermal strain). The magnitude of E depends on the quality of inter-splat/inter-layer adhesive bonding[63]. The quality of bonding strength at interfaces is a direct index of coating's integrity, toughness and yield strength, which can be also considered as practical criteria for durability and service life performance of SPS ceramic coatings in application involving wear and erosion [73].

Applied tensile strain during heating cycle induces embedded defects and layers interfaces to move, which cause coating exhibits its transition from linear to non-linear behavior[60]. So, the second parameter, non-linear degree (ND), can be used as a relative scale and approximation to estimate the coating defect density and their degree of movement within coating structure based on designated thermal strain. It is important to remember that the ND is considered as a comparative degree to describe the coatings mechanical compliance and resilience at elevated temperature with respect to its initial stiffness [63]. In general, for a given E, a higher value of ND exhibit the higher strain tolerance and mechanical compliance of coating, which is suitable for TBC applications at high temperature [50].

The third parameter, degree of hysteresis, can also be used as an index for the defects density, and their frictional interfacial sliding which dissipates energy during thermal cycles [63]. The density of coating cracks, and also the coefficient of friction at crack surfaces govern the hysteresis degree. The disparity between heating and cooling curve depends on the number of defects interfaces that participate in the non-linear behavior of coating. In general, a higher interfaces density may result in increasing hysteresis response and strain tolerance of the coating [49].

In short, the three anelastic parameters, E, ND and HD are unique for a given coating, and a complete understanding of three anelasticity parameters could shed light on the defect density embedded in a coating, and their contribution in the coatings compliance response.

3. Results and discussion

As mentioned earlier, the objectives of this thesis are divided into two major sections that comprise manufacturing of suspension plasma sprayed YSZ coating deposited under different spraying parameters, and then evaluation of coatings anelasticity parameters through ECP measurements. So, in the first section of this chapter, six coatings microstructure and the effect of various spraying parameters related to plasma torch conditions includes gun raster speed, torch-substrate distance, plasma gas composition, power (enthalpy) and internal nozzle diameter on the coatings microstructural features will be discussed (See Fig. 3.1) . Different regions in suspension plasma sprayed YSZ coatings were recognized and labeled on SEM results in a similar way for all pictures to have a better comparison scale within the observed coating structures. Dense and overspray regions of YSZ, columnar features, oblique and segmentation cracks, and porosities are the main features in the produced coatings structure. In fact, the target of this part is to assess the effect of spraying parameters on the coatings structure and to select three coatings with distinguished microstructural attributes for further mechanical property evaluation through thermal cycling measurements.

In the next section of this chapter, the curvature-temperature responses of six coated samples produced with the three selected processing conditions (two samples for each condition) will be plotted and evaluated for further analysis. The anelastic parameters will be computed through transferring the required input parameters to the developed program written by Stony Brook University to calculate the elastic modulus (E), degree of nonlinearity (ND), and hysteresis degree (HD). The results of calculated anelastic parameters for two samples of each spraying parameters will be evaluated to assess the repeatability of ECP test. In the final step, the results of anelastic parameters will be compared based on the SEM images of coated samples to correlate the sensitivity of anelastic responses to the coatings structure and spraying parameters. In fact, it would be interesting to establish a relation between the effect of processing conditions and the coatings structure to their corresponding anelastic responses.

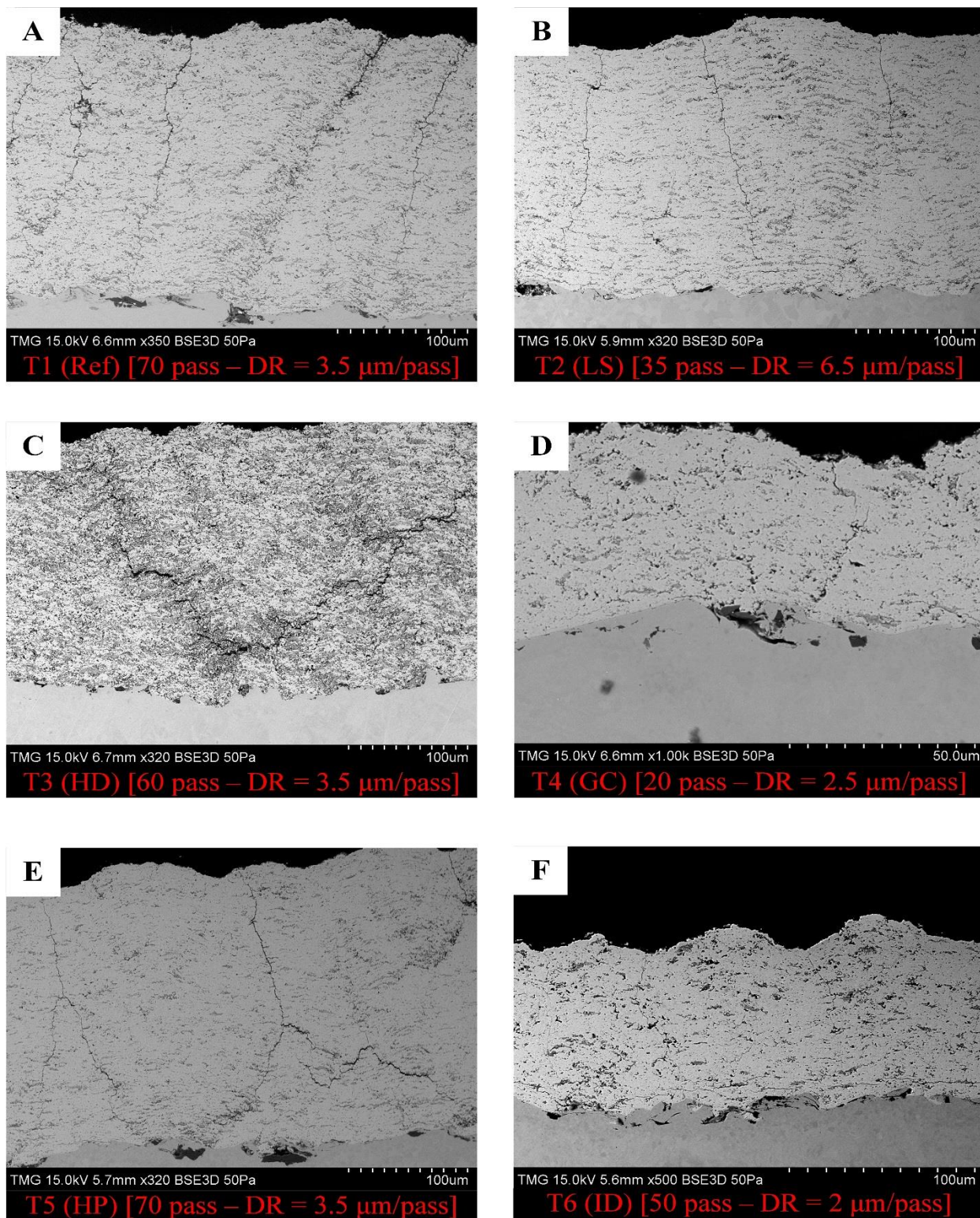


Figure 3-1 SEM pictures of six SPS YSZ coatings microstructure deposited under different spraying parameters. A) T1 (Ref). B) T2 (LS). C) T3 (HD). D) T4 (GC). E) T5 (HP). F) T6 (ID).

3.1. Suspension plasma sprayed YSZ coatings microstructure

It is well known that the process parameters can play a role on the deposition conditions meaning that, the deposition rate or degree of particles melting in a layer can be varied in each spraying process. The cross-section images of the sample of Test 1(Ref) which was sprayed with 70 passes with a 3.5 $\mu\text{m}/\text{pass}$ deposition rate (DR) was considered as a reference coating. Some microstructural characteristics of T1 (Ref), including segmentation cracks, porosities and dense/overspray deposits were observed at low and high magnification of SEM (See Fig. 3.2). The reason for segmentation cracks forming (“a”) can be related to the temperature gradient between substrate and coating during deposition. It is has been investigated that [31, 32] high-temperature gradient can result in the microcracks propagation trough the coating thickness which was formed initially by relaxation of tensile stress (quenching stress) during solidification. Columnar feature with inter-columnar voids which is related to the ‘shadow’ effect is also observed. As marked in the high magnification SEM image, dense (“b”) and overspray (“d”) deposited of YSZ within the coatings structure are evident. The dense regions are indicative of the particles that were well-treated in the center of the plasma plume in terms of thermal and kinetic energy. On the other hand, clusters of semi-molten or unmolten particles experienced less heat in the plasma periphery, deposited ahead or behind the fully molten particles on the substrate as overspray, and formed the YSZ coating with very fine pores. Also, some darker regions (“c”) are considered as pores. Their existence can be linked due to the incomplete contact between layers and improper adhesion (gas entrapment) during deposition.

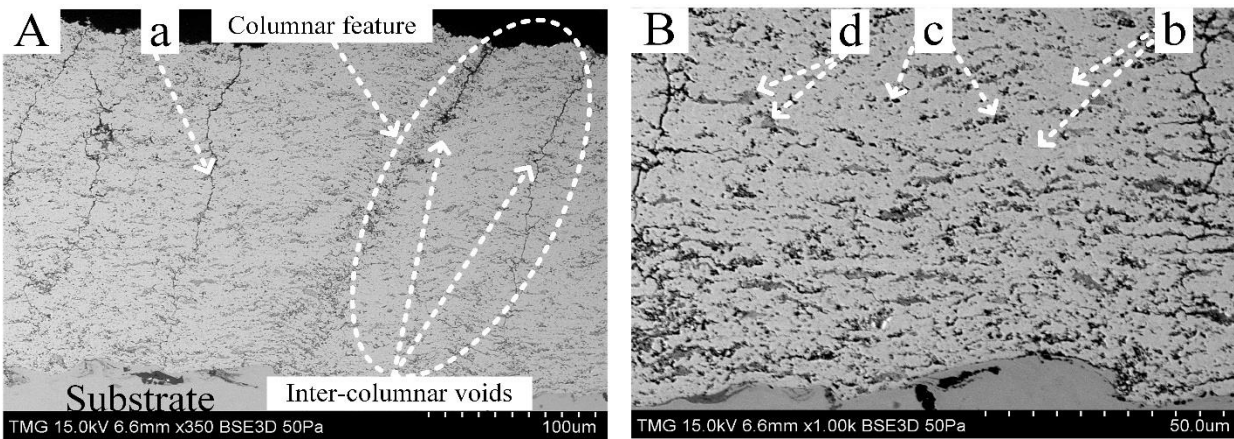


Figure 3-2. SEM pictures of SPS YSZ coating microstructure produced at T1 (Ref) condition. A) Low magnification with (a) segmentation cracks and columnar feature. B) High magnification with (b) dense regions of YSZ deposited (c) porosities (d) overspray regions of YSZ coating with very fine pores.

3.1.1. Effect of torch raster speed (LS)

In T2 (LS), all spraying parameters were similar compare to T1 (Ref), except the torch raster speed that decreased from 1m/s to 0.5m/s. The substrate was coated totally by 35 passes, with 6.5 $\mu\text{m}/\text{pass}$. From the low and high magnification images, different microstructural features (segmentation cracks, dense/overspray deposit of YSZ and porosities) can be observed as T1 coating microstructure. However, the most significant characteristic in T2 was the higher deposition rate than T1, and the formation of inter-pass boundaries in some regions of coating (See Fig. 3.3). The higher deposition rate can be directly related to lower speed in which more material (powder) can be deposited in a layer. Moreover, it is clear that since, at lower robot travel speed, the dwell time of the plasma torch in front of the substrate increases, the heat transfer from plasma to the substrate and deposited layers increases, thereby, cohesion degree of molten particles at the deposited bead might be improved. It can also be concluded that the local deposition temperature in lower torch raster speed would be higher, so it would result in better flattening and cohesion of molten particles in one layer. However, it can be suggested that the increased time interval between two consecutive deposited layers (Δt_{layer}) can result in forming the inter-pass boundaries, and consequently rather weaker adhesive bonding between passes. It is assumed that the mechanism behind the formation of such a coating can be correlated to the higher deposition rate in the center of deposited bead compared to its wings in one raster which can cause poor coating's layer-layer contact.

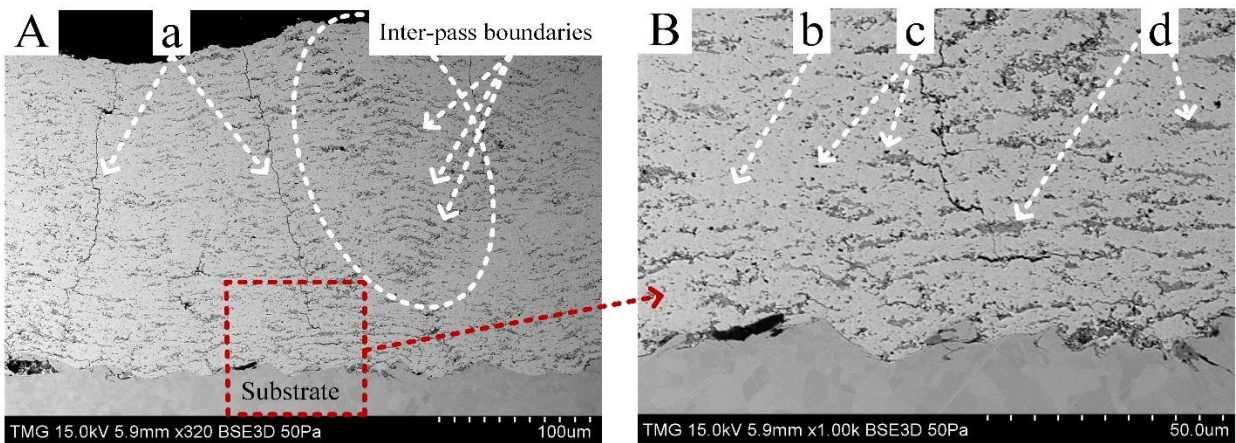


Figure 3-3. SEM pictures of SPS YSZ coating microstructure produced at low raster speed (LS) condition. A) Low magnification with (a) segmentation cracks and inter-pass boundaries. B) High magnification with (b) dense regions of YSZ deposited (c) porosities (d) overspray regions of YSZ coating with very fine pores are labeled.

3.1.2. Effect of torch-substrate distance (stand-off distance) (HD)

Compared to T1 spraying parameters, the torch-substrate distance increased from 30 mm to 50 mm at condition T3 (HD). The YSZ coating was performed by 60 passes with 3.5 $\mu\text{m}/\text{pass}$. The deposition rate was not changed, but the total porosity varied significantly compared to reference condition (See Fig. 3.4). From two aspects, the coating microstructure with relatively high stand-off distance (T3) can be analyzed. It should be noted that, since submicron particles have low thermal and kinetic inertia, they will reach the plasma gas velocity once they penetrate into the plasma plume, but they will lose their initial states (temperature and velocity) rapidly while increasing the stand-off distance. So, one can conclude that the local deposition temperature decreased, firstly due to the lower temperature of deposited particles which should travel a longer distance to impact, flatten and solidify on the substrate, and secondly, because of lower heat fluxes imparted from plasma jet to the substrate. It can be mentioned that, the consequence of longer spray distances is that, the main regions of YSZ coating microstructure are comprised of overspray particles (“d”) formed YSZ coating with very fine pores. The other characteristic which can be observed through investigation of SEM images is that when the distance increased, some agglomerated particles which well-treated in the plasma plume or those traveled in the jet fringes (semi-molten state) started to re-solidify during flight before impact which can be led to powdery deposit within coating structure in the spheroid shape. These re-solidified particles are labeled with the red circles (“e”).

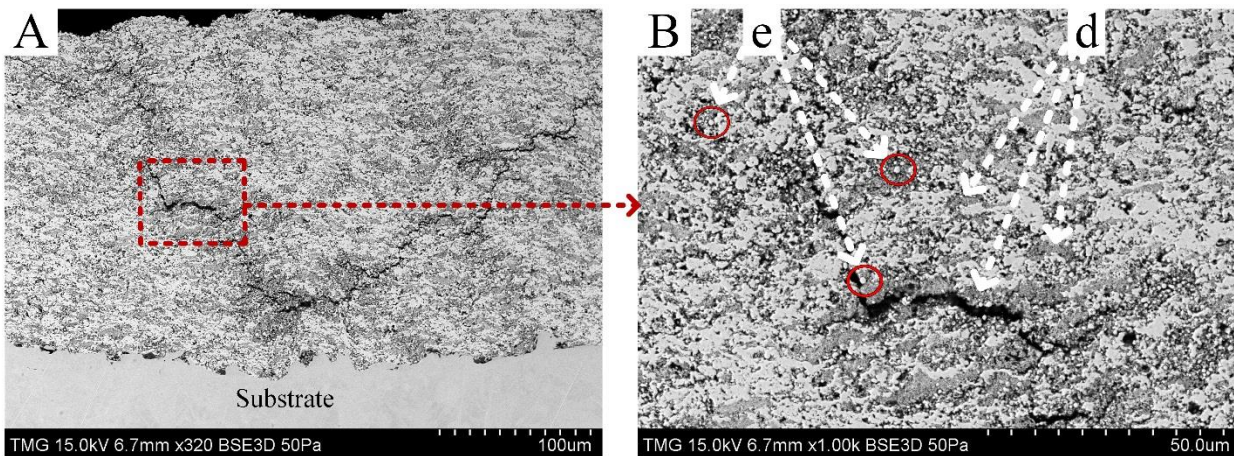


Figure 3-4. SEM pictures of SPS YSZ coating microstructure produced with high stand-off distance at (HD) condition. A) Low magnification with high density of overspray particles formed YSZ coating very fine pores. B) High magnification with (d) overspray regions of YSZ coating with very fine pores, and (e) re-solidified particles in the spheroid form embedded in the coating structure marked by red circles.

3.1.3. Effect of plasma gas composition (GC)

Plasma gas composition was replaced from Ar/He (25/25slpm) to Ar/H₂ (45/5 slpm) at condition T3 (GC). The coating was built-up by 20 passes with deposition rate 2 μm per pass. The reduction in deposition rate can be discussed through observed phenomena in suspension injection penetration and its interaction with plasma jet and coating quality can be analyzed by investigation on the plasma power and enthalpy generated with Ar/H₂ gas mixture. It has been shown that, through changing the plasma gas mixture from Ar/He to Ar/H₂, the arc voltage fluctuations were increased, and an increase in voltage fluctuations led to an increase in gas velocity variation. By means of a fast shutter camera, a decrease in suspension penetration depth, and an increase in suspension dispersion angle within the plasma plume were also observed [12,16,19]. So, according to the results of these previous researches, it is assumed that in this operating condition, the fragmentation was less efficient and occurred more in the jet fringes. Thereby, the small agglomerated particles which have low inertia were ejected from the plasma jet. Thereby, this can result in a reduction of propelled particles toward the substrate, and consequently deposition rate. In terms of coating quality, it should be noted that, using hydrogen as an auxiliary gas increases plasma voltage, and therefore plasma enthalpy and heat flux [74, 75]. As a result, it can be expected that the substrate was exposed to a higher thermal load due to higher heat transfer rates with H₂ than He. High magnification SEM observation suggested that those particles which were injected successfully into the plasma jet and treated close to the plasma core achieved enough thermal and kinetic energy to built-up a relative dense YSZ coating (See Fig. 3.4).

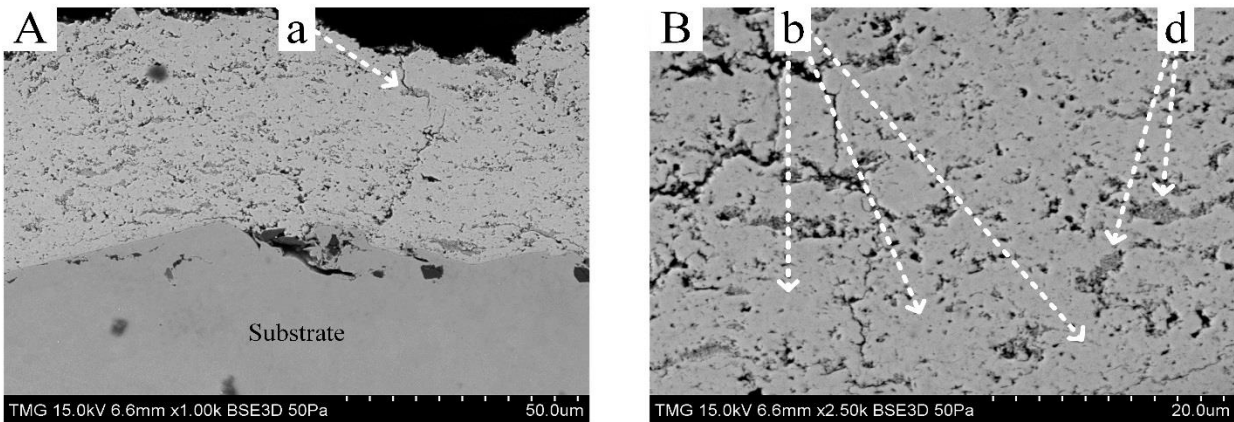


Figure 3-5. SEM pictures of SPS YSZ coating microstructure produced with Ar/H₂ plasma gas composition at (GC) condition. A) Low magnification with (a) segmentation crack started to initiate due to temperature gradient. B) High magnification with (b) dense regions and (d) overspray regions of YSZ coating with very fine pores.

3.1.4. Effect of current and plasma power (HP)

In T5 (HP), the current intensity and plasma power were increased to 700 Amp and 28kW, respectively. The coating was sprayed totally by 70 passes with 3.5 $\mu\text{m}/\text{pass}$. Compare to T1 (Ref), the deposition rate was not changed. Simple visual observation in low and high magnification of coating cross-section suggests that more dense structure obtained with condition T5 compared to T1 (See Fig. 3.5). The reason behind this structure can be correlated to the higher particle temperature, velocity, and substrate temperature through increasing plasma power. It has been shown that, through increasing the current and plasma power, particle temperature and velocity increased significantly [74–78]. So, according to this hypothesis, it can be expected that with spraying parameter at T5 (HP), injected particles exposed to higher plasma gas velocity which would result in increased impact velocity and improved contact between flattened layers. Also, it is clear that through increasing current and plasma power, the enthalpy of plasma plume increased which could be led to high degree of particles melting during deposition. Therefore, it can be expected that the enhanced bonding among layers and improved microstructure at T5 (HP) compared to a coating made with T1 (Ref) can be achieved. The presence of segmentation cracks within coating structure also suggested that, the quenching stress happened due to the temperature gradient between flattened particles and substrate. It should be reminded that, the segmentation crack structure is favored for TBC application since they provide strain tolerance for YSZ layers, and increase the coating compliance with the substrate at elevated temperature.

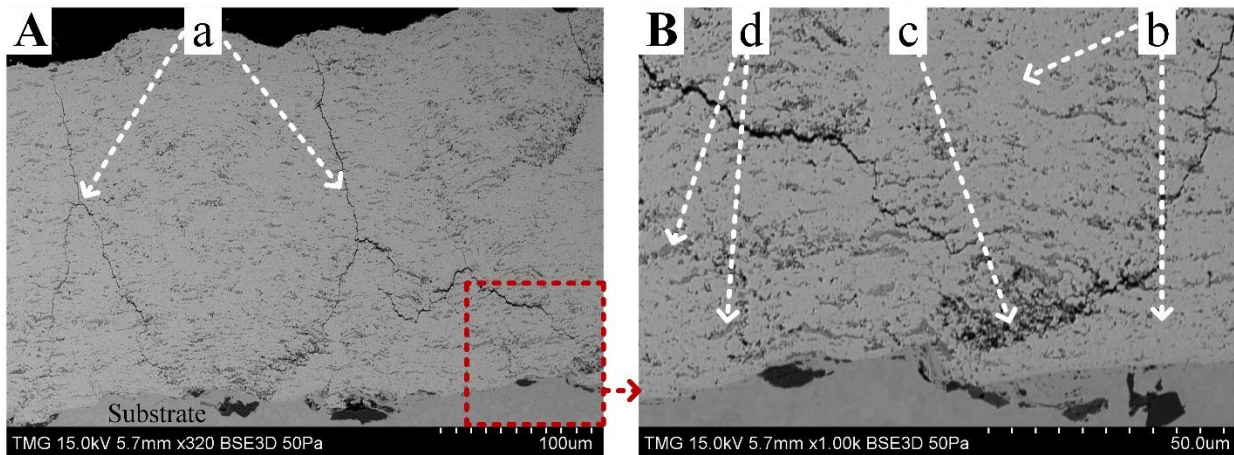


Figure 3-6. SEM pictures of SPS YSZ coating microstructure produced with high power at (HP) condition. A) Low magnification with (a) segmentation crack. B) High magnification with (b) dense regions of YSZ deposited (c) porosities (d) overspray regions of YSZ coating with very fine pores.

3.1.5. Effect of internal nozzle diameter (ID)

In the last run T6 (ID), the plasma gun internal nozzle diameter was changed from 5mm to 8mm. The coating was sprayed by 50 passes, and with 2 $\mu\text{m}/\text{pass}$. It is clear that, in the constant condition of plasma gas flow rate, the plasma gas velocity decreases through increasing the plasma gun cross section. This reduction in the gas velocity can influence the particles trajectories and treatment within the plasma plume. It can be suggested that the drop in the deposition rate at T6 spraying conditions compared to T1 correlated to those small particles with low velocity which were ejected radially from the plasma plume before impacting on the substrate, then fewer particles propelled toward the substrate. However, the lower particles velocity can result in an increased particles temperature, possibly due to a longer residence time of the particles treated in the plasma jet. Although these well-treated particles can ensure the layers bonding strength in a pass, its seems due to lack of enough particles impact velocity a poor contact area between layers in two consecutive passes occurred which resulted in the formation of relative long oblique crack (“f”) near to the substrate. These horizontal cracks are deleterious and can be led to the delamination between the coatings layers (See Fig. 3.6). The presence of segmentation cracks (“a”) in the low magnification SEM suggested that the particles with higher temperature impact to the substrate with lower local substrate temperature (larger projected area of plasma plume on the substrate) resulting in increasing the quenching stress (tensile stress), and consequently the segmentation crack propagation. The existent porosities (“c”) can also be related to the incomplete contact between layers during coating formation, and more air trapped in two consecutive rasters.

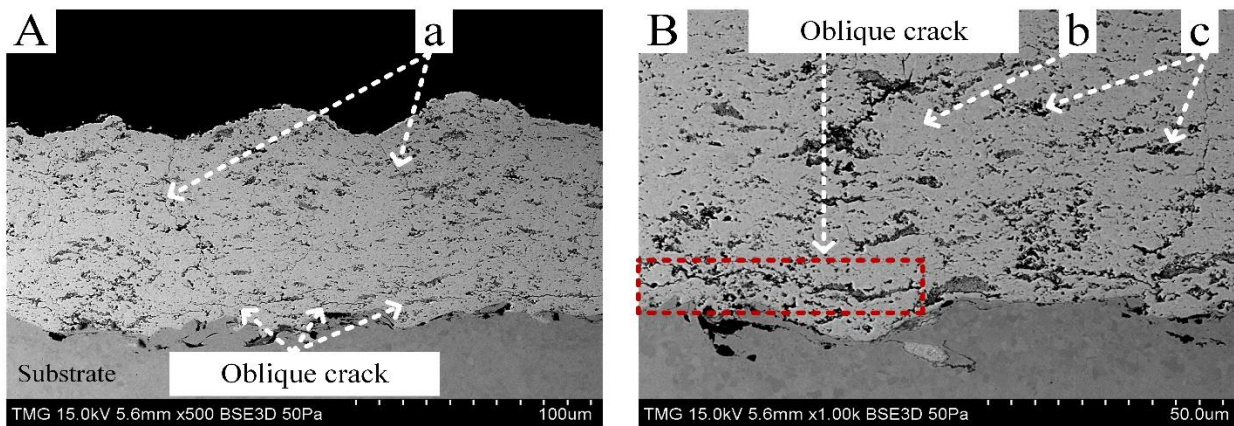


Figure 3-7 SEM pictures of SPS YSZ coating microstructure produced with larger internal nozzle diameter at (ID) condition. A) Low magnification with (a) segmentation crack. B) High magnification with (b) dense regions of YSZ deposited (c) porosities and (f) oblique crack due to poor bonding strength between layers in two consecutive passes.

3.2. Design of experiments for ex-situ coating property (ECP) process

After evaluation the SEM cross-section of six SPS YSZ coatings manufactured on small samples, three spraying parameters include T2 (low raster speed (LS)) with inter-pass boundaries pattern, T3 (high stand-off distance (HD)) with high level of overspray and very fine pores, and T5 (high power (HP)) with dense and segmentation crack structure exhibited distinct microstructure were selected (See Fig. 3.8).

To implement the thermal cycling test through ECP sensor, and to assess the repeatability analysis of anelastic parameters of coated samples, for each set of selected spraying parameter two samples (totally six samples) were sprayed on 304 stainless-steel with the rectangular shape of 230 mm x 25.4 mm x 1.5 mm.

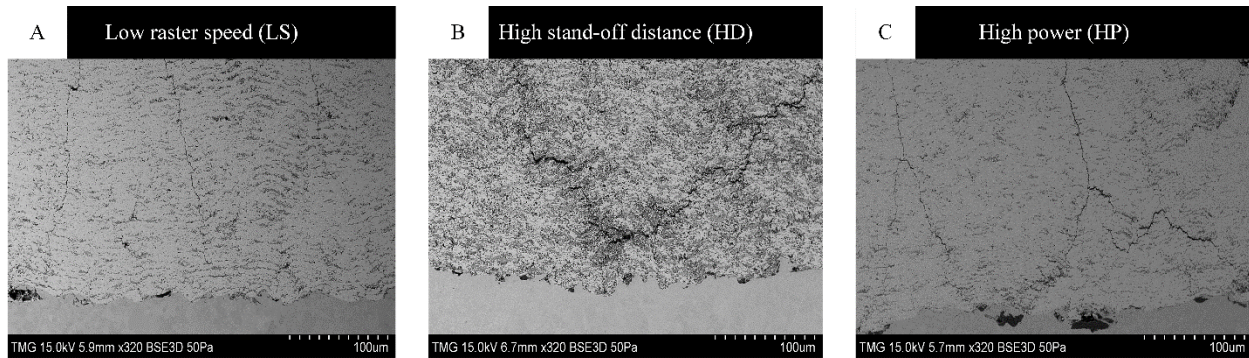


Figure 3-8. Three different SEM pictures of SPS YSZ coating microstructure. A) Lower raster speed (LS) with inter-pass boundaries structure. B) High stand-off distance (HD) with considerable porous regions. C) High power (HP) with denser region than (LS) condition comprising segmentation cracks within its structure.

It has been observed [79, 80] that the substrate surface temperature during thermal spray deposition played a critical role on the yttria stabilized zirconia (YSZ) coating structure and properties.

In order to evaluate the possible effect of deposition temperature on the coatings microstructure, and corresponded anelasticity parameters, the substrate temperature was measured during deposition. For each spraying parameters, specific temperature range was observed during deposition (See Fig. 3.9). Highest temperature was recorded in the case of lower raster speed (0.5 m/s) at T2 (LS) condition since the plasma gun passed across the substrate surface in longer time compared to two other cases. Also, the lowest substrate temperature was achieved when the stand-off distance was 50 mm at T3 (HD) condition. In T5 (HP) condition, although increasing current intensity and plasma power increased the enthalpy of the plume and substrate temperature; however, lower substrate temperature range was recorded compared to the LS condition. The effect

of the substrate temperature for each spraying condition on the coatings microstructure and analyzed anelasticity parameters will be discussed in details.

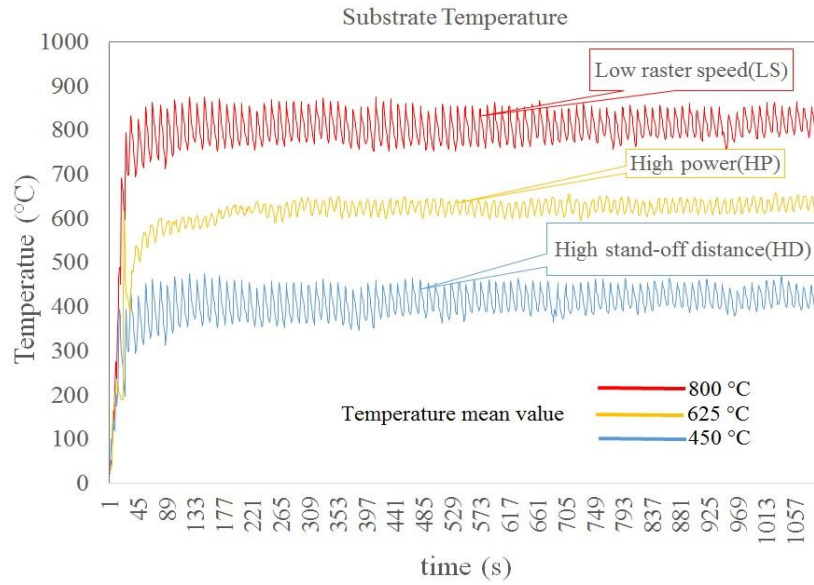


Figure 3-9. Substrate temperature measurement for different spraying parameters through attaching the thermocouple on the back side of the substrate.

3.3. Anelastic parameters and curvature-temperature responses

Through thermal cycles in ECP sensor, the coating-substrate system undergoes a curvature change due to thermal expansion mismatch between coating and substrate. In general, curvature changes depend on the coating and substrate thickness, strain changes ($\Delta\varepsilon = \Delta\alpha \times \Delta t$), and also the elastic modulus of the coating and substrate.

Multiple thermal cycling were performed for each coated samples to evaluate and analyze their curvature-temperature responses and related anelastic parameters. The results of each spraying condition will be discussed separately, and then they will be compared to each other to assess the sensitivity of ECP responses, and anelastic parameters to the spraying conditions.

Similar to any other measurement technique, the computation and quantification of anelastic parameters from ECP sensor can be erroneous if the required input parameters such as coating and substrate thickness are off by some percentage. Therefore, to evaluate the coating thicknesses distribution and to provide precise results for quantification of anelastic parameters, the coatings thicknesses close to the middle and the edge of the samples were measured under microscope. It was observed that, due to deposition raster pattern used in this study, the central part of coated

samples are thicker than its wings (See Fig. 3.10). The coating thickness average was measured through the method of weighted arithmetic mean, as the central part had higher portion than the edges.

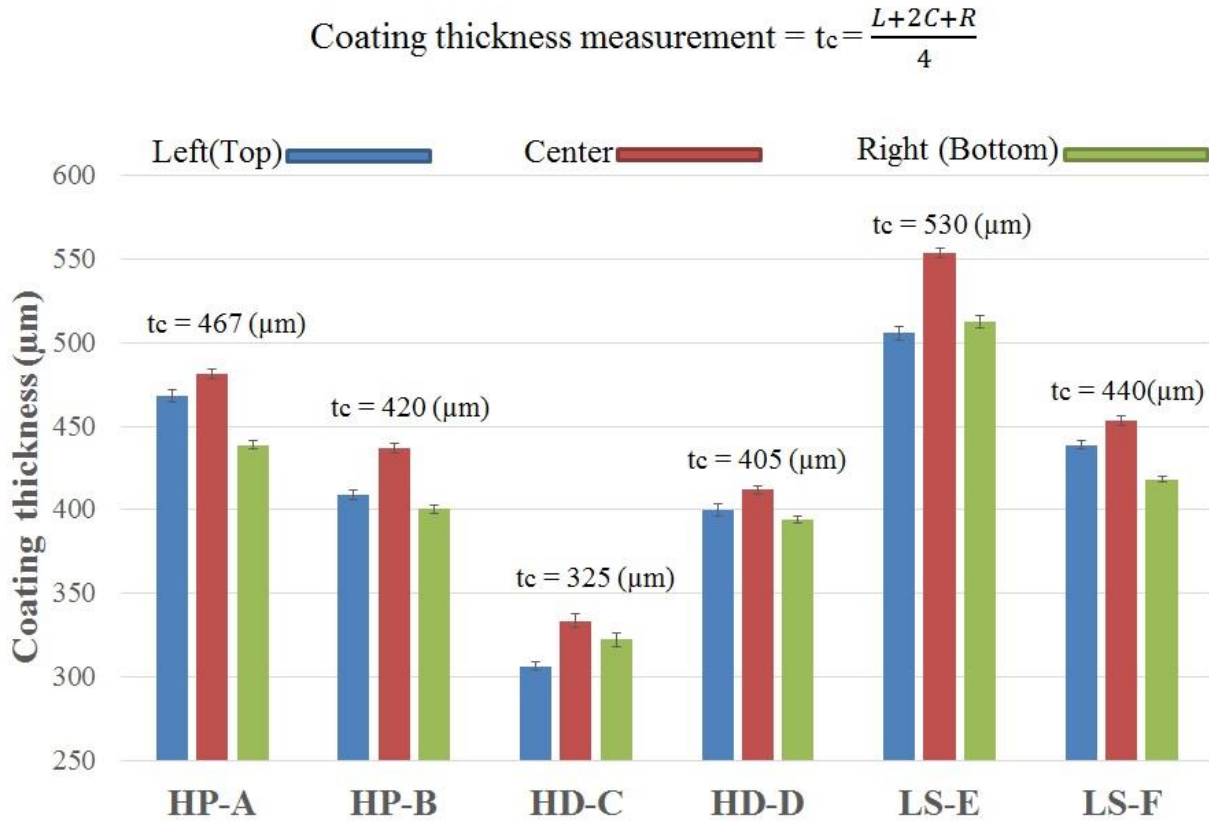


Figure 3-10. Coating thickness measurement for different samples (HP-A, HP-B, HD-C, HD-D, LS-E, and LS-F). The central parts are thicker than the edges in all samples due to higher overlapping density in the central zone.

3.3.1. High power (HP)

Two coated samples (A and B) were exposed to several thermal cycles from room temperature to 570°C, and their curvature-temperature responses were plotted separately. (See Fig. 3.10). Generally, the data of the first cycles is not included for the analysis of anelastic parameters as this specific response is a phase during which the system adjust itself and its behavior is not similar to the other cycles. Also, as it can be observed from the plotted curves, in some thermal cycles there are some uneven paths during heating and cooling, which is related to the laser intensity reduction through the accumulation of moisture, dust, or even water drops on the lasers window cause

disturbing the acquired curvature data. As discussed, to analyze the curvature-temperature responses, the heating part of those cycles exempting from any noise were selected to compute the elastic modulus (E) or initial stiffness of coating, and its degree of nonlinearity (ND) (See Table 3.1)

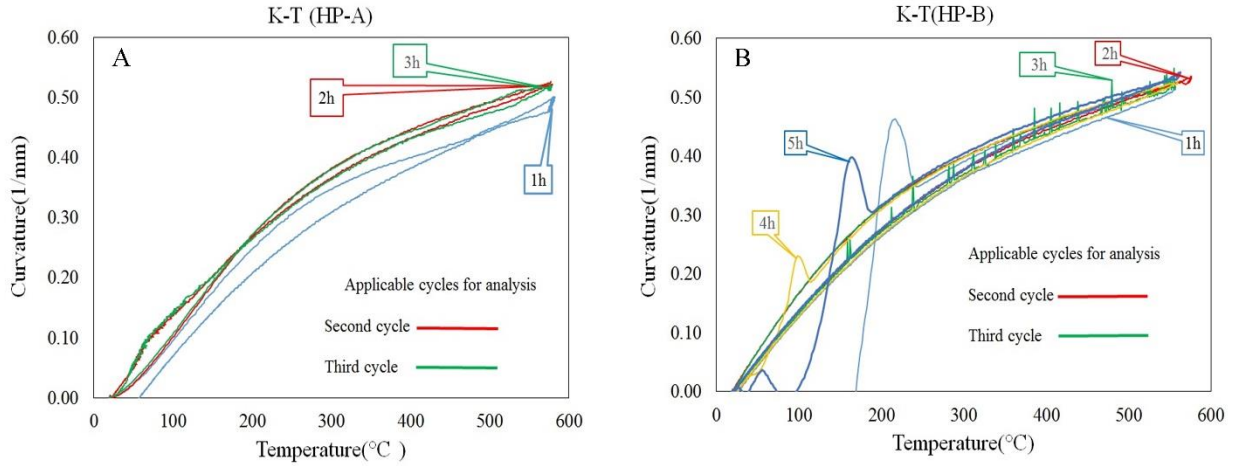


Figure 3-11 Curvature-temperature responses of SPS YSZ at high power (HP) condition. A) Second (2h) and third (3h) cycle of sample A, and B) Second (2h) and third (3h) cycle of sample B are qualified for analysis.

Table 3-1. Anelastic parameters of SPS YSZ in high power (HP) condition.

High Power (HP)	A		B	
	2h	3h	2h	3h
E (GPa)	58	55	93	94
ND	3.15	2.91	3.24	3.47
HD (%)	0.147	0.704	3.63	5.28

Although sample A and B produced in the same spraying conditions, their elastic modulus and hysteresis degree (HD) are significantly different. However, their degree of nonlinearity is quite in the same range. To provide a better description regarding the anelastic parameters, the corresponding coating microstructures were investigated which will be discussed in section 3.5.

It should be noted that a program developed by Stony Brook University was applied to calculate the hysteresis degree of curvature-temperature response, in which the heating and cooling curve did not intersect each other, and followed the regular pattern of air plasma spray (See Fig. 3.11).

According to the program, the calculated HD for the case of sample A (second and third cycles) divided into two section of positive and negative values related to the parts in which heating curve is up and down of cooling curve, respectively. Such a positive and negative pattern has just been seen in the case of SPS coating. The reason behind such an intersecting response is unknown at this point. As mentioned earlier, the values of HD can be used to explain the relative amount of energy dissipation in the coating structure during heating and cooling cycles originating from frictional sliding of embedded defects and internal interfaces in the coating structure. In fact, the coating's defects density have a direct relation with corresponding hysteresis degree. In short, it is not possible to compare and assess the HD values of curvature-temperature responses in which the heating and cooling part intersect each other to those exhibited the regular pattern of thermal cycling.

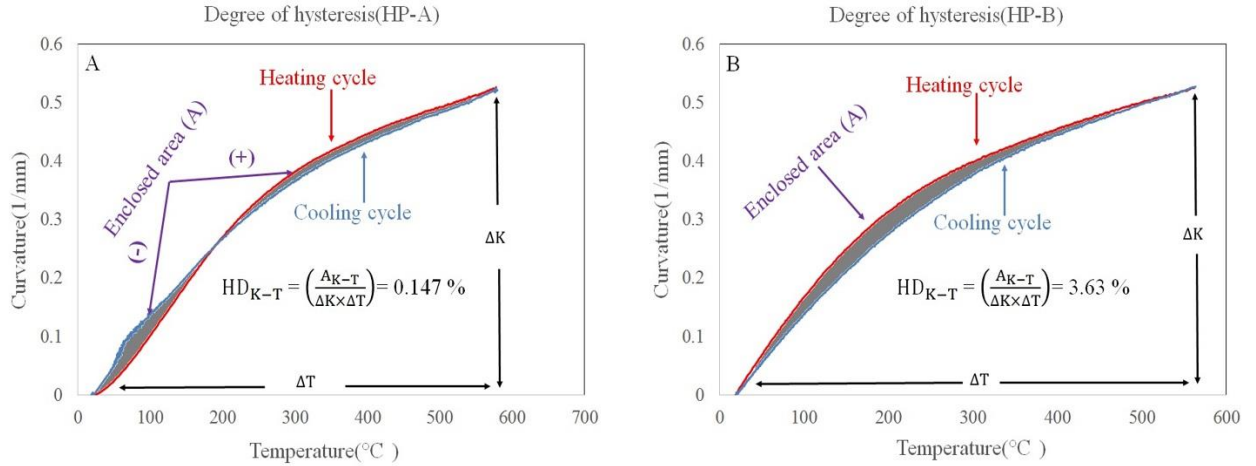


Figure 3-12. Calculation of hysteresis degree (HD). A) Second thermal cycle (2h) of sample A disregarding the hysteresis pattern of regular plasma spray and B) second thermal cycle (2h) of sample B following the hysteresis pattern of a regular plasma spray.

3.3.2. High stand-off distance (HD)

Similar to HP condition, several thermal cycles were executed for the samples C and D coated in high stand-off distance (HD) condition. The acquired data of curvature and temperature responses were plotted for each sample separately (See Fig. 3.12). In this case, all thermal cycles were included for anelastic parameters analysis (See Table 3.2).

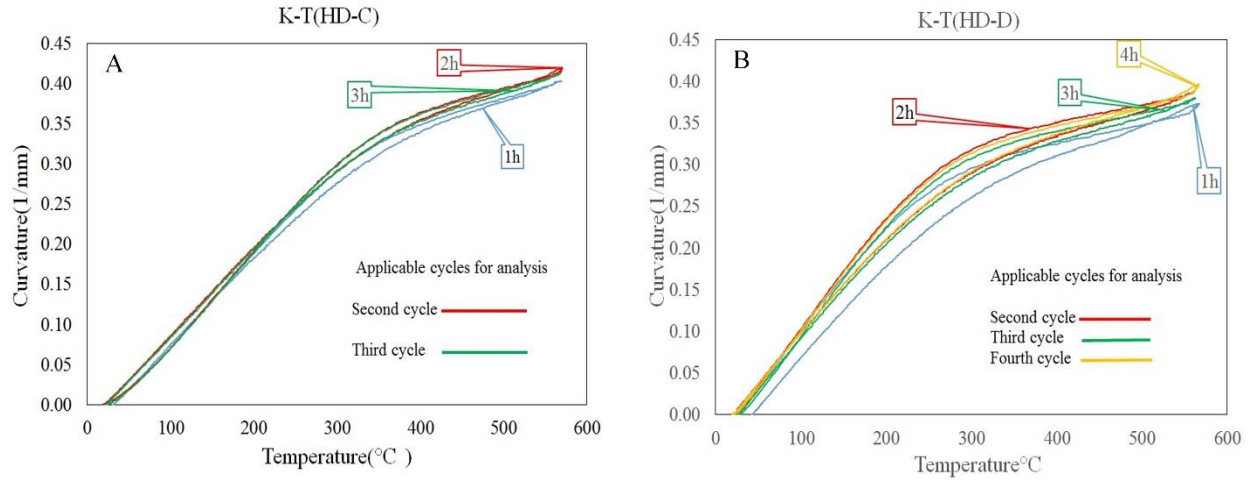


Figure 3-13. Curvature-temperature responses of SPS YSZ at high stand-off distance (HD) condition. A) Second (2h) and third (3h) cycle of sample C, and B) second (2h), third (3h) and fourth (4h) cycle of sample D are qualified for analysis.

Table 3-2. Anelastic parameters of SPS YSZ in high stand-off distance (HD) condition.

High stand-off distance (HD)	C		D		
	2h	3h	2h	3h	4h
E(GPa)	48	50	49	49	48
ND	3.07	3.22	3.7	3.22	3.35
HD (%)	0.304	0.125	3.77	2.94	2.53

Two samples in all cycles exhibited a narrow distribution regarding elastic modulus, and degree of nonlinearity (ND). The curvature-temperature responses in sample C had the same behavior as sample A in HP condition in which the cooling part during returning to room temperature cross the heating part. Therefore, the calculated hysteresis degree was very close to zero in this condition. It should be mentioned that, in terms of comparison hierarchy after elastic modulus and nonlinear degree measurement, the hysteresis degree value can be considered as a third anelastic parameter to assess the repeatability of ECP test.

3.3.3. Low raster speed (LS)

To assess the repeatability of ECP sensor on the curvature-temperature responses and the anelastic parameters, more thermal cycles were performed on the coated samples (E and F) compared to other conditions (See Fig. 3.14). As previous, anelastic parameters were analyzed on heating cycles without noisy patterns (See table 3.3).

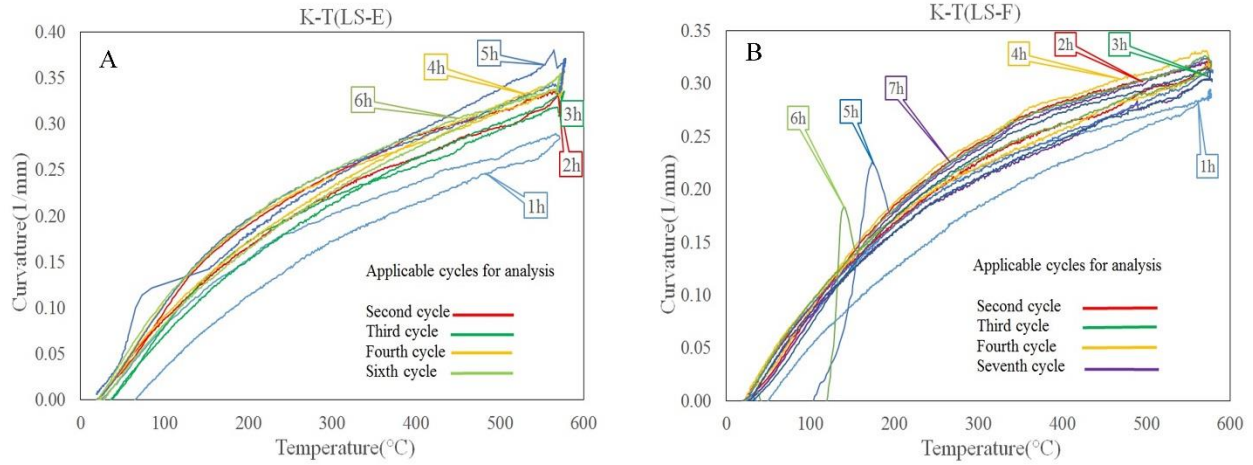


Figure 3-14. Curvature-temperature responses of SPS YSZ at low raster speed (LS) condition. A) Second (2h) third (3h), fourth (4h), and sixth (6h) cycle of sample E, and B) second (2h), third (3h), fourth (4h) and seventh (7h) cycle of sample F are qualified for analysis.

Table 3-3. Anelastic parameters of SPS YSZ in low raster speed (LS) condition.

Low raster speed (LS)	E				F			
	2h	3h	4h	6h	2h	3h	4h	7h
E(GPa)	32	33	36	39	39	37	38	36
ND	3.23	3.14	3.11	2.93	2.7	2.95	2.54	2.81
HD (%)	5.08	1.06	1.63	4.73	3.52	5.5	4.85	3.68

Excluding the third (3h) and fourth (4h) cycle of sample E in which the heating and cooling parts intersect each other, all results of two samples in terms of elastic modulus, degree of nonlinearity, and hysteresis degree exhibiting almost similar ranges and narrow distribution.

In the following section, the sensitivity of anelastic parameters to the spraying condition, and their corresponding microstructure will be discussed.

3.4. Sensitivity of curvature-temperature responses to the spraying conditions

It is clearly observable that curvature-temperature curves under the BCT measurement test exhibited dissimilar responses for coatings manufactured under different spraying parameters (See Fig. 3.15). However, any interpretation based on the curvature-temperature plots could be erroneous, as these plots strongly depend on the coating thicknesses, which were not similar for all the coatings. Two observations can be made from the figures. First, the initial slopes of the curves for the coatings are not same, which indicate that the stiffness of the coatings is different. Second, all coatings exhibited different degree of hysteresis, i.e. the loop areas are different.

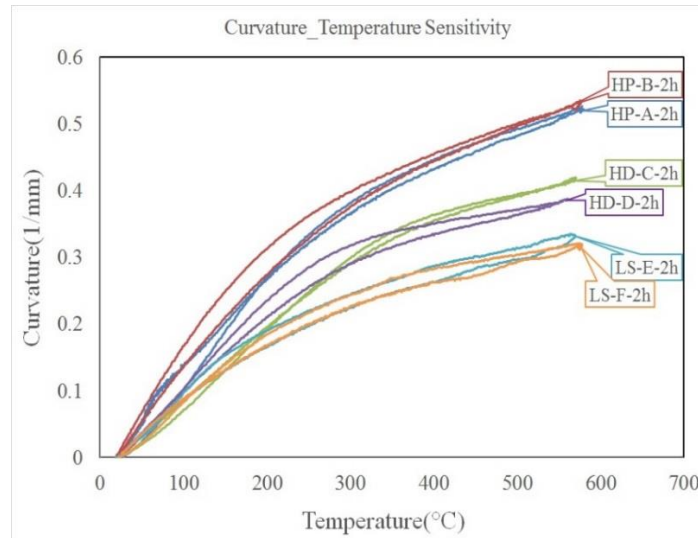


Figure 3-15. Curvature-temperature sensitivity to the spraying condition. The second cycle (2h) of all samples is selected to illustrate the sensitivity of curvature changes to the spraying condition under constant thermal strain ($\Delta\varepsilon = \Delta\alpha \times \Delta t$) for all samples.

3.5. Anelastic parameters of coatings and their corresponding microstructure

The map of non-linear elastic properties of SPS YSZ coatings demonstrating the sensitivity of anelastic parameters to the spraying condition (See Fig. 3.16). To make better description regarding the anelastic parameters, and corresponding spraying condition, the metallographic preparation were performed on the coated samples after ECP test to evaluate the coating formation pattern, and defects architecture based on their SEM images. (See Fig. 3.17)

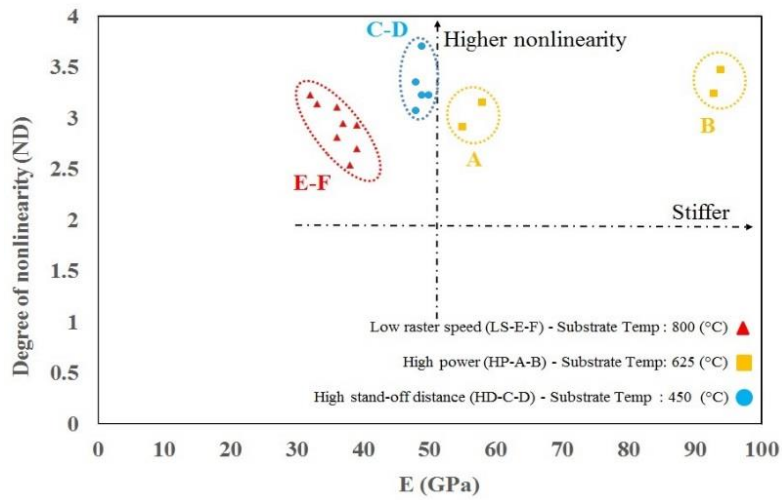


Figure 3-16. Map of non-linear elastic properties of SPS YSZ coatings to distinguish properties of various specimens manufactured in different spraying condition.

The elastic modulus of samples A and B produced in the same processing conditions (HP) exhibited significant differences. This can be related to the presence of the columnar feature and inter-columnar voids within the coating structure of sample A. Columnar feature developed from the asperities of the surface due to a shadow effect. In fact, the effect of shallow impact angle of particles leads to the formation of columnar feature and inter-columnar voids.

It should be noted that, during spraying for sample B, the suspension injector was clogged after a few passes and the plasma torch was stopped to replace another injector. The differences in their elastic modulus and coatings microstructure can be linked to the instability of SPS process during deposition of sample B. This observation showed the influence of consistency of SPS process during deposition on the repeatability of the coatings microstructure and its mechanical properties.

From SEM pictures of samples HP-A and HP-B and their corresponding elastic moduli, one can conclude that the high energy condition can result in a denser coating and consequently higher stiffness. Inter-splat/inter-layer adhesive bonding at HP condition would have been strong due to the higher melting degree and plasma enthalpy and this would mean that coating have relatively less amount of interfaces and defects between deposited layers. In fact, through increasing the current and plasma power, particles temperature and velocity increases, which cause improved impact velocity and contact between flattened particles. The measured temperature of mean value of local peak (625°C) in this condition suggested that the strong bonding within coatings structure can be produced in this temperature range.

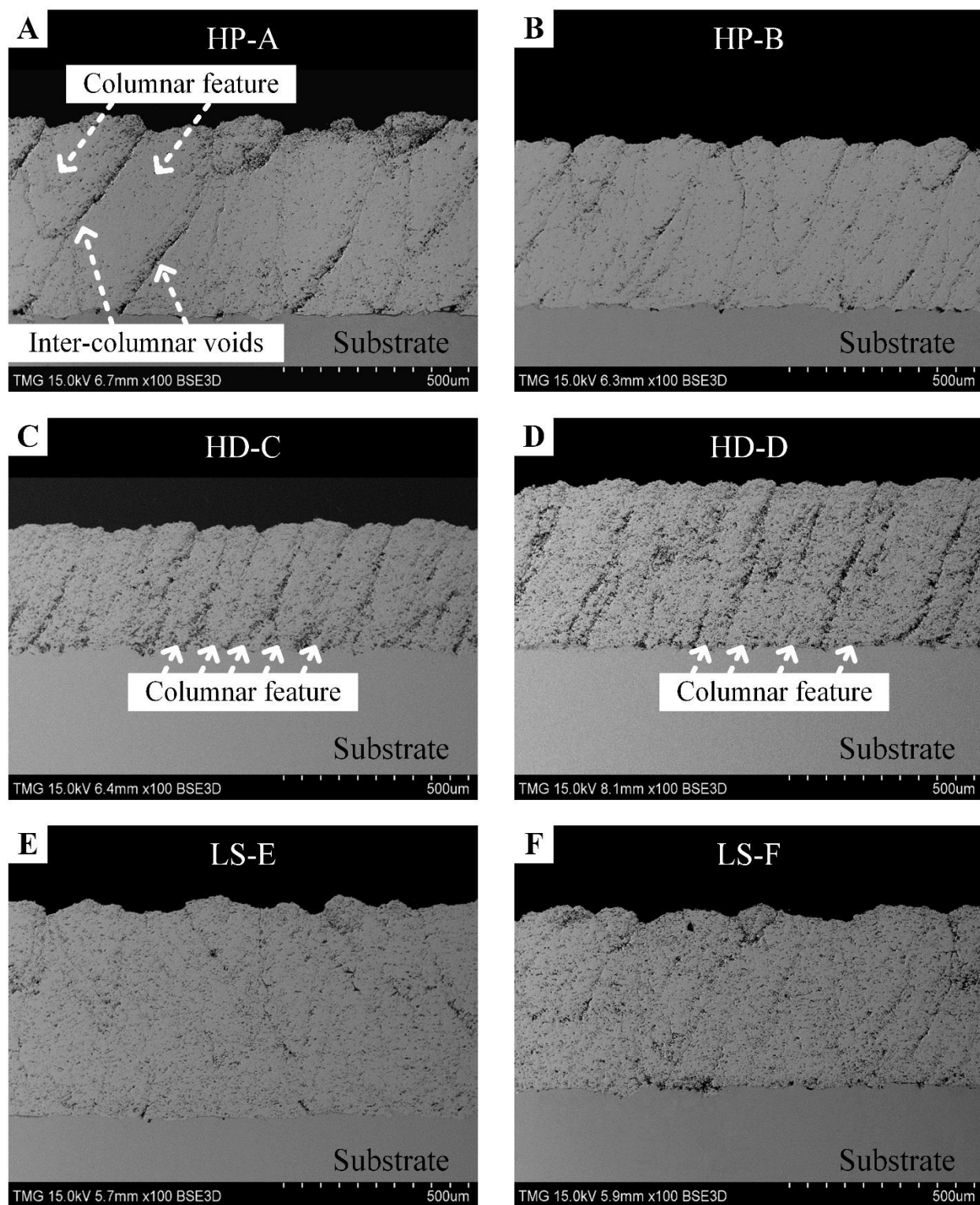


Figure 3-17. SEM pictures of six SPS YSZ coatings microstructure. A) and B) produced under high power condition (HP). C) and D) coated under high stand-off distance (HD) condition. E) and F) deposited under low raster speed (LS) condition.

To compare and assess the elastic modulus of samples E and F produced in LS condition with coated ones in HD condition, based on their microstructure, there are some facts which do not comply with the achieved results. It was expected at lower raster speed, the amount of material (powder) deposited per pass would be more, and moreover the local substrate deposition temperatures would be higher at the lower distance. Therefore, better flattening of splat in one layer and more dense coatings could be achieved. Moreover, it was presumed that the presence of columnar features with inter-columnar voids within coatings structure of samples C and D coated at higher stand-off distance could decrease coatings stiffness and integrity.

All indications mentioned above suggested that coatings produced in low raster speed (LS) condition should have had higher elastic modulus than coatings sprayed in high stand-off distance (HD) condition. Indeed, higher elastic moduli of samples C and D produced in HD condition than samples E and F coated at LS condition do not support their corresponding SEM pictures. To explain the higher values of elastic modulus of samples C and D produced in HD condition than LS ones, it should be emphasized that the measured elastic modulus through ECP sensor corresponds to the in-plane elastic modulus of sprayed coating (parallel to the coating surface). So, from this point of view to provide a reasonable judgment regarding the elastic modulus, the possible effects on the bonding quality between layers should be evaluated. There is two possible hypothesis related to the spraying condition which should be discussed separately.

The first one can be related to the time interval between two consecutive deposited layers (Δt_{layer}). It can be suggested that in lower raster speed, although the high local deposition temperature could result in strong bonding between splats in one layer (one pass), the increased Δt_{layer} due to lower plasma torch speed, and longer excursion of plasma torch in front of substrate during deposition of one layer decreased the bonding strength between two consecutive layers. Moreover, the reduced speed of plasma torch could play a role in the local temperature drop of previously deposited layer, and finally the adhesive bonding between two layers. In other words, although in HD condition the lowest local deposition temperature was recorded (450°C), the lower Δt_{layer} and higher raster speed than LS condition could provide a better layer-layer contact within coating structure.

The second possible hypothesis can be related to the coating deposition rate which can result in a different thickness of dense and porous region on the deposited bead. As discussed previously, the amount of deposited particles including molten particles those well-treated in the plasma plume, and semi-molten, or unmolten particles which were traveled in the plasma periphery can be variable based on applied processing conditions. The plasma torch raster speed can be considered as one of the most important parameters in suspension plasma spray which can alter the amount of deposited particles in one bead, and consequently the bonding strength between layers. Once the plasma torch scans the substrate surface, the molten particles form a dense region in the bead central part, while the poor-treated particles make a porous zone in the bead edges (See Fig. 3.18). The thickness of dense, and porous zone can be changed with respect to plasma torch raster speed, since it spends more or less time in front of the substrate. Therefore, it can be suggested that, in low raster speed condition the thickness of porous zone in one layer should be higher than high raster speed condition (See Sect. 2.3.3 for more details).

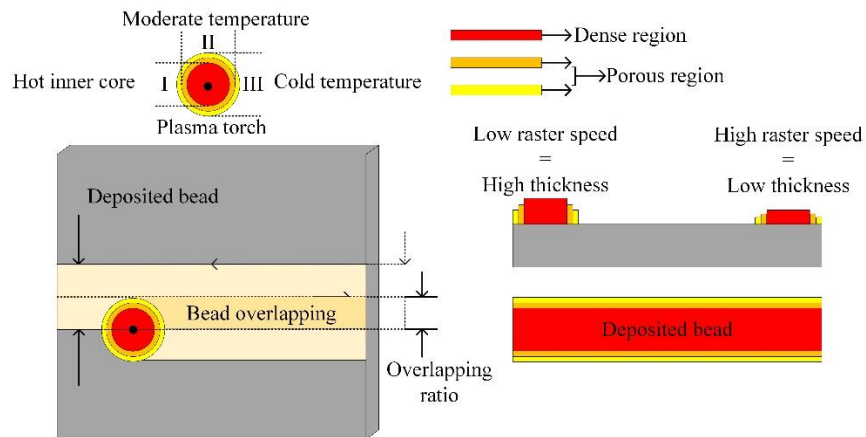


Figure 3-18. Coating deposition pattern, and the influence of plasma torch raster speed on the thickness of dense and porous zone of deposited bead.

Low raster speed and high deposition rate can be considered as the main principal reason for inter-pass boundaries and poor bonding strength of coating's layers which were observed at SEM picture at T2 (LS) condition (See Fig. 3.3.A). As these inter-pass boundaries were not detected in the SEM images of large samples produced in LS condition (E and F), one can suggest that these features might be affected during multiple thermal cycles at high temperature under ECP test. The reason behind this hypothesis is originated from the principle of anelasticity response of the plasma sprayed coatings which is attributed to the opening/closing of defects and interfaces movement at elevated temperature.

To support the proposed explanation, the small sample coated in T2 (LS) condition with inter-pass boundaries was taken out from the epoxy, and put in the furnace to simulate the thermal cycling of ECP procedure. The furnace was programmed to heat the sample up to 570°C for 40 min, and then left it to cool down inside the furnace. The procedure was performed for seven cycles to provide the exact condition of ECP method. After completion the multiple thermal cycles on small sample, it was molded into the epoxy, and polished again for SEM evaluation (See Fig. 3.19). Two different area (B, C) were selected to have a better judgment regarding the possible effect of thermal cycling on inter-pass boundaries. Through assessment of the SEM images, before and after thermal cycling, significant changes were not observed.

Since the coating is above the neutral axis during the bending, it can be suggested that coating's interfaces exerted a compressive force on each other during heating. However, the apparent poor zones of bonding between layers (white arrows in SEM image before thermal cycling) were not influenced effectively after seven times thermal cycling. It should be noted that the relative movement of splat/layer interfaces can be more perceptible on the large samples with higher coating thickness.

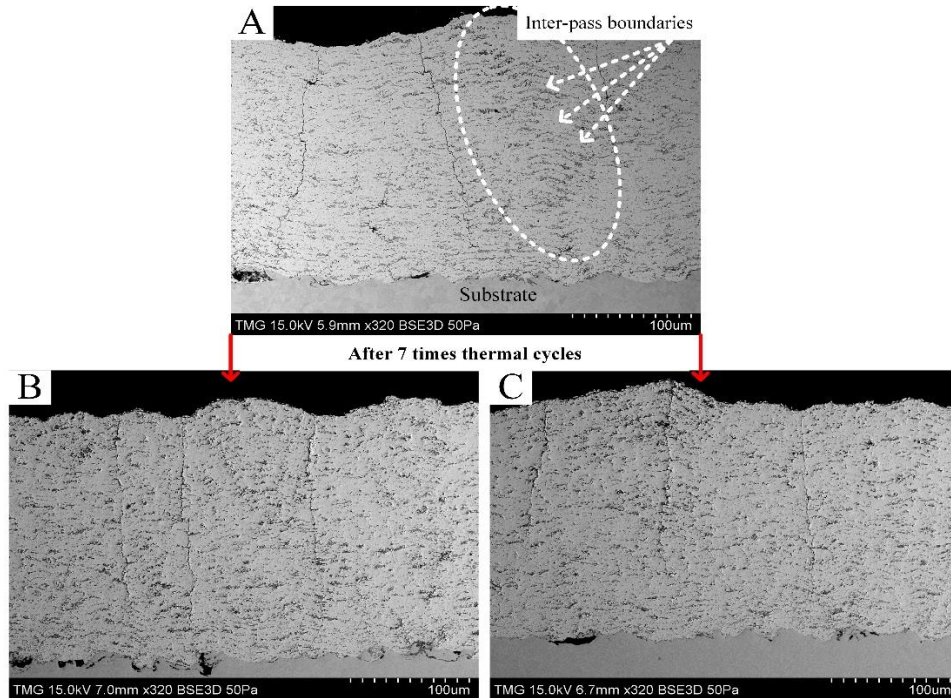


Figure 3-19. SEM pictures of SPS YSZ coating microstructure. A) Before thermal cycling with inter-pass boundaries. B) And C) after thermal cycling.

As mentioned previously, the magnitude of ND relates to the coating flexibility and compliance at elevated temperature with respect to its E value. So, the elastic modulus at low strain (E) and their corresponding secant modulus (E_{sec}) for each cycle is calculated (from Eq. (2.2). $ND = \left(\frac{E_c}{E_{sec}} \right)$) and plotted to provide a better understanding regarding the value of degree of non-linearity (See Fig. 3.20).

Coatings produced in LS condition exhibited lower elastic modulus at elevated temperature (E_{sec}) than other samples produced in HP and HD conditions. The lower secant elastic modulus can be attributed to the higher degree of sliding and opening/closure of defects, which results in softening of the coating structure at higher temperature. The higher secant modulus of samples A and B produced in HP condition is justifiable based on their SEM images. However, at this point, to establish a correlation between coatings compliance with their corresponding SEM images, it is necessary to measure the density of different types of defects (pores, micro-crack) in coatings structure, which is beyond the scope of the present study.

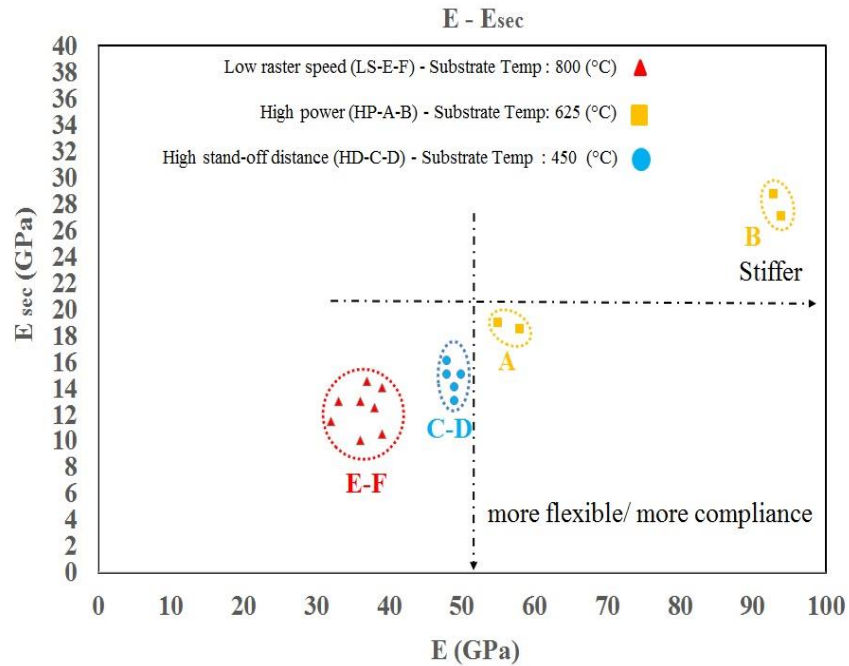


Figure 3-20. Map of elastic modulus (E) and secant modulus (E_{sec}) to distinguish the coatings compliance and flexibility.

3.6. Evaluation of elastic modulus of SPS YSZ coatings

As previously discussed, the elastic modulus of plasma sprayed coating is an index for inter-splat/inter-layer integrity at low strain. Coating's defects (e.g., pores, cracks, inter-column voids) affect the coating's stiffness and the quality of bonding within its lamellar structure. So, the quantification of elastic modulus at low strain (E) largely depends on the method of measurement and the contribution of coating's defects with respect to applied load (See table 3.3). For example, it has been shown that the elastic modulus of SPS YSZ was in the range of 100-170 GPa through nanoindentation test[81]. The high elastic modulus of SPS YSZ measured with the nanoindentation test can be explained by the limitation of local force applied on a specific area which induced the contribution of lower volume fraction of coating's defect in the measurement. In fact, this range of elastic modulus is close to the elastic modulus of pure YSZ (~ 200 GPa) at room temperature.

In another experiment, the elastic modulus of SPS YSZ free-standing coating (without substrate) was measured through three-point bending test [27]. The very low values of elastic modulus of three-point bending test compared to BCT measurement performed in this study can be described by the effect of substrate removal and coating's integrity reduction. It can be speculated that the coating-substrate interface can play role as a foundation for coating's build-up mechanism. Also, it can be proposed that the coating's lamellar structure will lose its integrity significantly, and it can be deformed more freely when the substrate is removed.

The bi-layer curvature-temperature (BCT) measurement apply more uniform stress along the samples without requiring the substrate removal. Moreover, through quantification of anelastic parameters, it is possible to estimate the coating's compliance and flexibility at high strain when the coating's defects and internal interfaces begin to movement.

Table 3-4. Evaluation of elastic modulus of SPS YSZ coatings

Experimental procedure	Young's modulus of SPS at low strain (GPa)
Nanoindentation	100 - 170
Bi-layer curvature – temperature (BCT)	30 - 90
Three-point bending	3-5

4. Conclusion and future work

The first study discussed in this thesis was conducted to evaluate the effect of different suspension plasma spraying parameters on the YSZ coating microstructure. Through investigation of SEM images of coated samples, different microstructural features, including dense and overspray regions of YSZ, columnar features, inter-pass boundaries, oblique and segmentation cracks were recognized. In fact, in suspension plasma spray process, coatings features including segmentation crack, columns and pores are desirable structures to produce a coating with low thermal conductivity, high strain tolerance and thermal shock resistance at the elevated temperature for TBC application. It is noticeable that, among defined processing condition in this research, some coatings with columnar features and segmentation crack were observed.

Excluding samples A and B produced in high power condition (HP) in which the suspension was clogged for sample B, the reproducibility of SPS process regarding coatings microstructure for the same spray parameters was observed based on the SEM pictures of large coated samples in LS and HD condition. However, the SEM images of coatings microstructure of small samples observed in the first part of this study exhibited different features and structures compared to those sprayed on the large samples with the same processing conditions. The differences in coatings structure can be related to the geometry of substrate, the difference in day to day ambient conditions and the variability introduced due to start-stop of the plasma torch. Also, it should be mentioned that the suspension viscosity used for deposition on the small samples was 5.2 (mPa-s), while for spraying on the large samples, suspension with 4.2 (mPa-s) dynamic viscosity was used.

In the existing literature, there is an evident lack of studies focusing on the quantification of the anelastic parameters of suspension plasma sprayed ceramic coatings. Therefore, the second part of this thesis was dedicated to the evaluation of the anelastic behavior of three SPS YSZ coatings with significantly different microstructures through bi-layer curvature-temperature (BCT) measurements.

As mentioned above, without considering samples A and B produced at high power condition (HP), it can be concluded that the anelastic parameters (elastic modulus and degree of nonlinearity) for two coated samples at the same spraying conditions were repeatable.

However, the calculated hysteresis degree (HD) measurements were not repeatable and comparable as some curvature-temperature responses showed irregular behavior and intersected each other during thermal cycling. The reasons for this kind of curvature-temperature responses in which the heating and cooling curves intersect each other during thermal cycling are still not understood and need to be investigated in more detail in future studies.

One of the main objectives of this study was to evaluate the effect of processing conditions on the anelastic behavior of suspension plasma sprayed YSZ coatings. It was observed that the coatings manufactured with high power (HP) condition had higher elastic modulus than other coatings which was correlated with the SEM images of coated samples. The higher elastic modulus was attributed to the stronger integrity of inter-splat/inter-layer due to higher particles impact velocity, and increased melting of the particles because of higher current intensity, and plasma enthalpy, respectively.

The shorter time interval between spraying two consecutive layers (Δt_{layer}) in high stand-off (HD) condition than low raster speed (LS) condition suggested the first possible reason for better inter-layer adhesion and coatings integrity in HD condition. The second possible reason for higher elastic modulus of the HD condition compared to the LS condition was attributed to the deposition rate and distribution of dense and porous regions on the deposited bead which can be variable with different raster speeds and can have an effect on the bonding strength of the coating's layers.

To establish a correlation between coatings compliance at elevated temperature and the degree of non-linearity with their corresponding microstructure, it is necessary to measure the density of different types of defects within coatings structure.

From the measured substrate temperature during deposition and the magnitudes of elastic modulus, it can be concluded that higher substrate temperature does not always support the better bonding strength between deposited layers. In fact, it can be proposed that the effect of spraying parameters such as plasma torch raster speed is more pronounced than local deposition temperature on the quality of bonding between layers. Also, it can be speculated that very high substrate temperature during deposition might enhance the residual stresses, which have a deleterious influence on coating inter-layer bonding.

For future work, to provide more reliable and applicable results regarding the anelastic behavior of suspension plasma spray YSZ coatings and to identify the effective processing conditions on the coatings structure, the following proposed studies can be considered:

- Investigate the effect of surface asperities and roughness on the coatings architecture and their corresponding anelastic parameters by using different sizes of grits for sandblasting, or through applying other methods of surface preparation such as high-pressure water jet roughening, abrasive water jet, and laser treatment.
- Evaluate the influence of the YSZ suspension concentration on the produced coating structures and mechanical properties. The suspension concentration influences its viscosity, surface tension, and density. Each of these parameters can play a role on the suspension interaction with the plasma plume and consequently on particles treatment and coating microstructure.
- To verify the ECP results, apply some other techniques of young's modulus measurement such as, 3 and 4 points bending test, and laser-ultrasonic technique which is based on surface acoustic waves (SAWs) or Rayleigh waves to analyze and evaluate the behavior of in-plane elastic modulus of thermally sprayed coatings.
- To match the actual service temperature of TBCs application, the ECP test can be performed at higher temperature to assess the behavior of microstructural features at a much higher and dynamic strain rates.
- To better understand the relationship between the coating structure and anelasticity, it would be interesting to better quantify the density of defects (pores, cracks, inter-column voids, etc.) by image analysis and mercury intrusion porosimetry.
- It is worth to mention that, SPS YSZ coatings produced in this research exhibited higher stiffness at low temperature, and degree of nonlinearity at high temperature than those deposited on aluminum substrate through air plasma spray (APS) process at Stony Brook University, NY, USA (See Fig. 4.1). As a future work, it would be more applicable from industrial approach to produce different YSZ coatings with APS and SPS process with the same coating thickness and similar substrate, and to quantify their anelastic parameters through bi-layer curvature-temperature (BCT) measurements under same conditions. In fact, it would be interesting to evaluate the effect of different spraying parameters of both APS and SPS on the bonding strength of inter-splat/inter-layer at low strain, and also to

investigate their compliance and degree of nonlinearity at similar temperature range under ECP sensor.

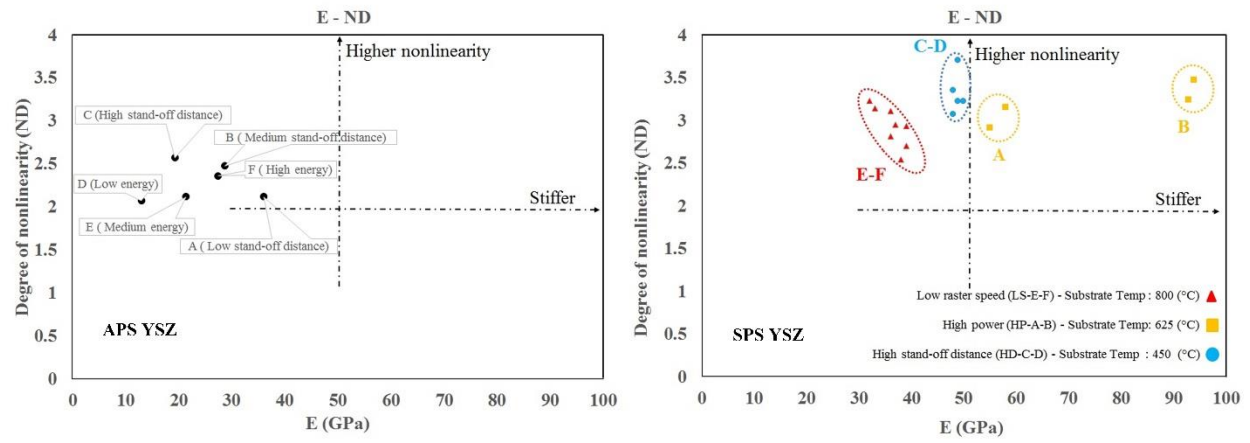


Figure 4-1. Maps of non-linear elastic properties of YSZ coated through air plasma spray (left), and suspension plasma spray (right).

References

- [1] R. F. Bunshah, *HANDBOOK OF DEPOSITION TECHNOLOGIES and Applications*, Second. Published in the United States of America by Noyes Publications, 1994.
- [2] P. M. Martin, “Thin Film Deposition Processes,” in *Introduction to Surface Engineering and Functionally Engineered Materials*, John Wiley & Sons, Inc., 2011, pp. 39–141.
- [3] P. L. Fauchais, J. V. R. Heberlein, and M. I. Boulos, *Thermal Spray Fundamentals*. 2014.
- [4] L. Pawlowski, *The science and engineering of thermal spray coatings*, vol. 34. 1995.
- [5] W. Handbook, C. Committee, and W. Handbook, “Thermal spraying and cold spraying,” in *AWS WELDING HANDBOOK, Volume 3, chapter 11*, pp. 367–419.
- [6] C. C. Koch, *Nanostructured Materials: Processing, Properties and Applications - Second Edition*. 2007.
- [7] P. Fauchais, G. Montavon, R. S. Lima, and B. R. Marple, “Engineering a new class of thermal spray nano-based microstructures from agglomerated nanostructured particles, suspensions and solutions: an invited review,” *J. Phys. D. Appl. Phys.*, vol. 44, no. 9, p. 093001, 2011.
- [8] N. B. Dahotre and S. Nayak, “Nanocoatings for engine application,” *Surf. Coatings Technol.*, vol. 194, no. 1, pp. 58–67, 2005.
- [9] Y. Lu and P. Liaw, “The mechanical properties of nanostructured materials,” *Jom*, vol. 53, no. 3, pp. 31–35, 2001.
- [10] M. Gell, “Application opportunities for nanostructured materials and coatings,” *Mater. Sci. Eng. A*, vol. 204, pp. 246–251, 1995.
- [11] P. G. Klemens, “Theory of Thermal Conduction in Thin Ceramic Films,” *Int. J. Thermophys.*, vol. 22, no. 1, pp. 265–275, 2001.
- [12] P. Fauchais and A. Vardelle, “Solution and Suspension Plasma Spraying of Nanostructure Coatings,” *Adv. Plasma Spray Appl.*, pp. 149–188, 2012.
- [13] Z. Chen, R. W. Trice, M. Besser, X. Yang, and D. Sordet, “Air-plasma spraying colloidal solutions of nanosized ceramic powders,” *J. Mater. Sci.*, vol. 39, no. 13, pp. 4171–4178, 2004.
- [14] D. Damiani, D. Tarlet, and E. Meillot, “A Particle-Tracking-Velocimetry (PTV) Investigation of Liquid Injection in a DC Plasma Jet,” *J. Therm. Spray Technol.*, vol. 23, no. 3, pp. 340–353, 2013.
- [15] R. Siegert, “A Novel Process for the Liquid Feedstock Plasma Spray of Ceramic Coatings with Nanostructural Features,” 2005.
- [16] R. Etchart-Salas, V. Rat, J. F. Coudert, P. Fauchais, N. Caron, K. Wittman, and S. Alexandre, “Influence of Plasma Instabilities in Ceramic Suspension Plasma Spraying,” *J. Therm. Spray Technol.*, vol. 16, no. 5–6, pp. 857–865, 2007.
- [17] P. Fauchais, V. Rat, C. Delbos, J. F. Coudert, T. Chartier, and L. Bianchi, “Understanding

- of suspension DC plasma spraying of finely structured coatings for SOFC,” *IEEE Trans. Plasma Sci.*, vol. 33, no. 2, pp. 920–930, 2005.
- [18] S. Selle and U. Riedel, “Transport properties of ionized species,” *Annals of the New York Academy of Sciences*, vol. 891, 1999.
 - [19] P. Fauchais, R. Etchart-Salas, V. Rat, J. F. Coudert, N. Caron, and K. Wittmann-Ténèze, “Parameters Controlling Liquid Plasma Spraying: Solutions, Sols, or Suspensions,” *J. Therm. Spray Technol.*, vol. 17, no. 1, pp. 31–59, 2008.
 - [20] C. G. Levi, “Emerging materials and processes for thermal barrier systems,” *Curr. Opin. Solid State Mater. Sci.*, vol. 8, no. 1, pp. 77–91, 2004.
 - [21] A. Feuerstein, J. Knapp, T. Taylor, A. Ashary, A. Bolcavage, and N. Hitchman, “Technical and Economical Aspects of Current Thermal Barrier Coating Systems for Gas Turbine Engines by Thermal Spray and EBPVD: A Review,” *J. Therm. Spray Technol.*, vol. 17, no. 2, pp. 199–213, 2008.
 - [22] U. Schulz, C. Leyens, K. Fritscher, M. Peters, B. Saruhan-Brings, O. Lavigne, J. M. Dorvaux, M. Poulain, R. Mévrel, and M. Caliez, “Some recent trends in research and technology of advanced thermal barrier coatings,” *Aerosp. Sci. Technol.*, vol. 7, no. 1, pp. 73–80, 2003.
 - [23] H. Kassner, R. Siegert, D. Hathiramani, R. Vassen, and D. Stoever, “Application of Suspension Plasma Spraying (SPS) for Manufacture of Ceramic Coatings,” *J. Therm. Spray Technol.*, vol. 17, no. 1, pp. 115–123, 2008.
 - [24] K. VanEvery, M. J. M. Krane, R. W. Trice, H. Wang, W. Porter, M. Besser, D. Sordet, J. Ilavsky, and J. Almer, “Column Formation in Suspension Plasma-Sprayed Coatings and Resultant Thermal Properties,” *J. Therm. Spray Technol.*, vol. 20, no. 4, pp. 817–828, 2011.
 - [25] N. Curry, K. Vanevery, T. Snyder, J. Susnjar, and S. Bjorklund, “Performance Testing of Suspension Plasma Sprayed Thermal Barrier Coatings Produced with Varied Suspension Parameters,” pp. 338–356, 2015.
 - [26] J. Matejcek, S. Sampath, P. C. Brand, and H. J. Prask, “Quenching, thermal and residual stress in plasma sprayed deposits: NiCrAlY and YSZ coatings,” *Acta Mater.*, vol. 47, no. 2, pp. 607–617, 1999.
 - [27] A. Guignard, G. Mauer, R. Vaßen, and D. Stöver, “Deposition and characteristics of submicrometer-structured thermal barrier coatings by suspension plasma spraying,” *J. Therm. Spray Technol.*, vol. 21, no. 3–4, pp. 416–424, 2012.
 - [28] R. S. Lima and B. R. Marple, “Toward highly sintering-resistant nanostructured ZrO₂-7wt.%Y₂O₃ coatings for TBC applications by employing differential sintering,” *J. Therm. Spray Technol.*, vol. 17, no. 5–6, pp. 846–852, 2008.
 - [29] P. Fauchais, R. Etchart-Salas, C. Delbos, M. Tognonvi, V. Rat, J. F. Coudert, and T. Chartier, “Suspension and solution plasma spraying of finely structured layers: potential application to SOFCs,” *J. Phys. D. Appl. Phys.*, vol. 40, no. 8, pp. 2394–2406, 2007.
 - [30] R. McPherson, “Plasma Sprayed Ceramic Coatings,” vol. 40, pp. 173–181, 1989.
 - [31] N. Curry, K. VanEvery, T. Snyder, and N. Markocsan, “Thermal Conductivity Analysis

- and Lifetime Testing of Suspension Plasma-Sprayed Thermal Barrier Coatings,” *Coatings*, vol. 4, no. 3, pp. 630–650, 2014.
- [32] M. Karger, R. Vaßen, and D. Stöver, “Atmospheric plasma sprayed thermal barrier coatings with high segmentation crack densities: Spraying process, microstructure and thermal cycling behavior,” *Surf. Coatings Technol.*, vol. 206, no. 1, pp. 16–23, 2011.
 - [33] H. B. Guo, R. Vaßen, and D. Stöver, “Atmospheric plasma sprayed thick thermal barrier coatings with high segmentation crack density,” *Surf. Coatings Technol.*, vol. 186, no. 3, pp. 353–363, 2004.
 - [34] Z. Wang, a. Kulkarni, S. Deshpande, T. Nakamura, and H. Herman, “Effects of pores and interfaces on effective properties of plasma sprayed zirconia coatings,” *Acta Mater.*, vol. 51, no. 18, pp. 5319–5334, 2003.
 - [35] T. Nakamura, G. Qian, and C. C. Berndt, “Effects of Pores on Mechanical Properties of Plasma-Sprayed Ceramic Coatings,” *J. Am. Ceram. Socety*, vol. 83, pp. 578–584, 2000.
 - [36] L. Łatka, A. Cattini, L. Pawłowski, S. Valette, B. Pateyron, J.-P. Lecompte, R. Kumar, and A. Denoirjean, “Thermal diffusivity and conductivity of yttria stabilized zirconia coatings obtained by suspension plasma spraying,” *Surf. Coatings Technol.*, vol. 208, pp. 87–91, 2012.
 - [37] L. Łatka, L. Pawłowski, D. Chicot, C. Pierlot, and F. Petit, “Mechanical properties of suspension plasma sprayed hydroxyapatite coatings submitted to simulated body fluid,” *Surf. Coatings Technol.*, vol. 205, no. 4, pp. 954–960, 2010.
 - [38] J. Oberste Berghaus, J.-G. Legoux, C. Moreau, F. Tarasi, and T. Chráska, “Mechanical and Thermal Transport Properties of Suspension Thermal-Sprayed Alumina-Zirconia Composite Coatings,” *J. Therm. Spray Technol.*, vol. 17, no. 1, pp. 91–104, 2008.
 - [39] S. Sampath, X. Y. Jiang, J. Matejcek, L. Prchlik, a. Kulkarni, and a. Vaidya, “Role of thermal spray processing method on the microstructure, residual stress and properties of coatings: An integrated study of Ni-5 wt. % Al bond coats,” *Mater. Sci. Eng. A*, vol. 364, pp. 216–231, 2004.
 - [40] F. Kroupa and J. Plešek, “Nonlinear elastic behavior in compression of thermally sprayed materials,” *Mater. Sci. Eng. A*, vol. 328, no. 1, pp. 1–7, 2002.
 - [41] F. Kroupa and J. Dubský, “Pressure dependence of Young’s moduli of thermal sprayed materials,” *Scr. Mater.*, vol. 40, no. 11, pp. 1249–1254, 1999.
 - [42] W.-Z. Wang, C.-J. Li, Y.-Y. Wang, G.-J. Yang, and K. Sonoya, “Tensile deformation behavior of plasma-sprayed Ni–45Cr coatings,” *Surf. Coatings Technol.*, vol. 201, no. 3–4, pp. 842–847, 2006.
 - [43] T. Wakui, J. Malzbender, and R. W. Steinbrech, “Strain Analysis of Plasma Sprayed Thermal Barrier Coatings Under Mechanical Stress,” *J. Therm. Spray Technol.*, vol. 13, no. 3, pp. 390–395, 2004.
 - [44] C. P. Development, “Mechanical Properties/Database of Plasma-Sprayed ZrO₂-8wt% Y₂O₃ Thermal Barrier Coatings,” vol. 71, pp. 161–171, 2004.
 - [45] E. F. Rejda, D. F. Socie, and T. Itoh, “Deformation behavior of plasma-sprayed thick thermal barrier coatings,” *Surf. Coatings Technol.*, vol. 113, no. 3, pp. 218–226, 1999.

- [46] R. Bott, "Quasistatic VS. Dynamic modulus measurements of plasma-sprayed thermal barrier coatings," *Igarss 2014*, no. 1, pp. 1–5, 2014.
- [47] M. Arai, X. Wu, and K. Fujimoto, "Inelastic Deformation of Freestanding Plasma-sprayed Thermal Barrier Coatings," *J. Solid Mech. Mater. Eng.*, vol. 4, no. 2, pp. 221–234, 2010.
- [48] V. Harok and K. Neufuss, "Elastic and inelastic effects in compression in plasma-sprayed ceramic coatings," *J. Therm. Spray Technol.*, vol. 10, no. 1, pp. 126–132, 2001.
- [49] Y. Liu, T. Nakamura, G. Dwivedi, A. Valarezo, and S. Sampath, "Anelastic behavior of plasma-sprayed zirconia coatings," *J. Am. Ceram. Soc.*, vol. 91, no. 12, pp. 4036–4043, 2008.
- [50] G. Dwivedi, T. Nakamura, and S. Sampath, "Controlled introduction of anelasticity in plasma-sprayed ceramics," *J. Am. Ceram. Soc.*, vol. 94, pp. 104–111, 2011.
- [51] Y. Liu, T. Nakamura, V. Srinivasan, A. Gouldstone, and S. Sampath, "Mechanism Underlying Anelastic Properties of Thermal Spray Coating Temperature (C)," *New York*, pp. 225–229, 2007.
- [52] G. Stoney, "The tension of metallic films deposited by electrolysis," 1909.
- [53] G. Carlotti, L. Doucet, and M. Dupeux, "Elastic properties of silicon dioxide films deposited by chemical vapour deposition from tetraethylorthosilicate," *Thin Solid Films*, vol. 296, no. 1–2, pp. 102–105, 1997.
- [54] V. Lacquaniti, E. Monticone, and G. B. Picotto, "Structural and surface properties of sputtered Nb films for multilayer devices," *Surf. Sci.*, vol. 377–379, pp. 1042–1045, 1997.
- [55] P. Krulevitch, P. B. Ramsey, D. M. Makowiecki, A. P. Lee, M. A. Northrup, and G. C. Johnson, "Mixed-sputter deposition of Ni-Ti-Cu shape memory films," *Thin Solid Films*, vol. 274, no. 1–2, pp. 101–105, 1996.
- [56] B. Hunsche, M. Vergöhl, H. Neuhäuser, F. Klose, B. Szyszka, and T. Mattheé, "Effect of deposition parameters on optical and mechanical properties of MF- and DC-sputtered Nb₂O₅ films," *Thin Solid Films*, vol. 392, no. 2, pp. 184–190, 2001.
- [57] Y. Oka, M. Tao, Y. Nishimura, K. Azuma, E. Fujiwara, and M. Yatsuzuka, "Properties of thick DLC films prepared by plasma-based ion implantation and deposition using combined RF and H.V. pulses," *Nucl. Instruments Methods Phys. Res. Sect. B Beam Interact. with Mater. Atoms*, vol. 206, pp. 700–703, 2003.
- [58] S. Menzel, S. Strehle, H. Wendrock, and K. Wetzig, "Effect of Ag-alloying addition on the stress–temperature behavior of electroplated copper thin films," *Appl. Surf. Sci.*, vol. 252, no. 1, pp. 211–214, 2005.
- [59] T. Nakamura and Y. Liu, "Determination of nonlinear properties of thermal sprayed ceramic coatings via inverse analysis," *Int. J. Solids Struct.*, vol. 44, no. 6, pp. 1990–2009, 2007.
- [60] Y. Liu, T. Nakamura, V. Srinivasan, a. Vaidya, a. Gouldstone, and S. Sampath, "Non-linear elastic properties of plasma-sprayed zirconia coatings and associated relationships with processing conditions," *Acta Mater.*, vol. 55, pp. 4667–4678, 2007.
- [61] G. Dwivedi, T. Nakamura, and S. Sampath, "Determination of thermal spray coating property with curvature measurements," *J. Therm. Spray Technol.*, vol. 22, pp. 1337–

1347, 2013.

- [62] G. Dwivedi, T. Wentz, S. Sampath, and T. Nakamura, "Assessing Process and Coating Reliability Through Monitoring of Process and Design Relevant Coating Properties," *J. Therm. Spray Technol.*, vol. 19, no. 4, pp. 695–712, 2010.
- [63] G. Dwivedi, "On the Anelastic Behavior of Plasma Sprayed Ceramic Coatings: Observations, Characterizations and Applications." Stony Brook University, 2011.
- [64] V. Viswanathan, "Effect of Processing Conditions on the Anelastic Behavior of Plasma Sprayed Thermal Barrier Coatings," 2011.
- [65] P. Fauchais, V. Rat, J.-F. Coudert, R. Etchart-Salas, and G. Montavon, "Operating parameters for suspension and solution plasma-spray coatings," *Surf. Coatings Technol.*, vol. 202, no. 18, pp. 4309–4317, 2008.
- [66] L. Pawlowski, "Suspension and solution thermal spray coatings," *Surf. Coatings Technol.*, vol. 203, no. 19, pp. 2807–2829, 2009.
- [67] R. Rampon, O. Marchand, C. Filiatre, and G. Bertrand, "Influence of suspension characteristics on coatings microstructure obtained by suspension plasma spraying," *Surf. Coatings Technol.*, vol. 202, no. 18, pp. 4337–4342, 2008.
- [68] J. Aubreton, M. F. Elchinger, P. Fauchais, V. Rat, and P. André, "Thermodynamic and transport properties of a ternary Ar–H₂–He mixture out of equilibrium up to 30 000 K at atmospheric pressure," *J. Phys. D. Appl. Phys.*, vol. 37, no. 16, pp. 2232–2246, Aug. 2004.
- [69] M. Gell, E. H. Jordan, M. Teicholz, B. M. Cetegen, N. P. Padture, L. Xie, D. Chen, X. Ma, and J. Roth, "Thermal Barrier Coatings Made by the Solution Precursor Plasma Spray Process," *J. Therm. Spray Technol.*, vol. 17, no. 1, pp. 124–135, 2008.
- [70] L. Xie, X. Ma, A. Ozturk, E. H. Jordan, N. P. Padture, B. M. Cetegen, D. T. Xiao, and M. Gell, "Processing parameter effects on solution precursor plasma spray process spray patterns," *Surf. Coatings Technol.*, vol. 183, no. 1, pp. 51–61, 2004.
- [71] P. Fauchais and G. Montavon, "Latest developments in suspension and liquid precursor thermal spraying," *J. Therm. Spray Technol.*, vol. 19, no. 1–2, pp. 226–239, 2010.
- [72] Y. Liu, "Anelastic Behavior of Thermal Spray Coatings and Associated Relationships with Processing Conditions," *Strain*, no. August, 2007.
- [73] J. Matejicek and S. Sampath, "In situ measurement of residual stresses and elastic moduli in thermal sprayed coatings part 1: Apparatus and analysis," *Acta Mater.*, vol. 51, no. 3, pp. 863–872, 2003.
- [74] D. Waldbillig and O. Kesler, "Effect of suspension plasma spraying process parameters on YSZ coating microstructure and permeability," *Surf. Coatings Technol.*, vol. 205, no. 23–24, pp. 5483–5492, 2011.
- [75] M. S. Morsi, S. a Abd, E. Gwad, M. a Shoeib, and K. F. Ahmed, "Effect of Air Plasma Sprays Parameters on Coating Performance in Zirconia – Based Thermal Barrier Coatings," *Int. J. Electrochem. Sci.*, vol. 7, pp. 2811–2831, 2012.
- [76] M. Prystay, P. Gougeon, and C. Moreau, "Structure of Plasma-Sprayed Zirconia Coatings Tailored by Controlling the Temperature and Velocity of the Sprayed Particles," *J. Therm.*

- Spray Technol.*, vol. 10, no. 1, pp. 67–75, 2001.
- [77] R. Vaen, H. Kaner, G. Mauer, and D. Stöver, “Suspension plasma spraying: Process characteristics and applications,” *J. Therm. Spray Technol.*, vol. 19, no. 1–2, pp. 219–225, 2010.
 - [78] K. Wittmann, F. Blein, M. F. J. Fazilleau, J. Coudert, P. Fauchais, and L. F., “A new process to deposit thin coatings by injecting nanoparticles suspensions in a DC plasma jet
Ein neuartiges Verfahren zur Herstellung von Dünnschichten durch Injektion von Nanopartikelsuspensionen in ein DC-Plasma,” no. 072538.
 - [79] J. Fazilleau, C. Delbos, M. Violier, J. Coudert, and P. Fauchais, “Influence of Substrate Temperature on Formation of Micrometric Splats Obtained by Plasma Spraying Liquid Suspension,” vol. 2, no. 072538, pp. 889–893, 2003.
 - [80] S. Sampath, X. . Jiang, J. Matejcek, A. . Leger, and A. Vardelle, “Substrate temperature effects on splat formation, microstructure development and properties of plasma sprayed coatings Part I: Case study for partially stabilized zirconia,” *Mater. Sci. Eng. A*, vol. 272, no. 1, pp. 181–188, 1999.
 - [81] P. Carpio, E. Bannier, M. D. Salvador, A. Borrell, R. Moreno, and E. Sánchez, “Effect of particle size distribution of suspension feedstock on the microstructure and mechanical properties of suspension plasma spraying YSZ coatings,” *Surf. Coatings Technol.*, vol. 268, pp. 293–297, 2015.